
High Pressure Gas Xenon TPCs for Double Beta Decay Searches

J.J. Gomez-Cadenas^{1,2,*}, F. Monrabal¹ and P. Ferrario^{1,2,*}

¹Donostia International Physics Center (DIPC), Spain.

²Ikerbasque, Spain.

Correspondence*:
Corresponding Author
jgomezcadenas@dipc.org

ABSTRACT

This article reviews the application of high pressure gas xenon (HPXe) time projection chambers to neutrinoless double beta decay experiments. First, the fundamentals of the technology and the historical development of the field are discussed. Then, the state of the art is presented, including the prospects for the next generation of experiments with masses in the ton scale.

Keywords: xenon, neutrinos, electroluminescence, resolution, topology, barium tagging, SMFI.

1 INTRODUCTION

The invention of the time projection chamber (TPC) [Nygren, 1974] revolutionized the imaging of charged particles in gaseous detectors. More than four decades after its introduction, the TPC is still one of the most important detectors in particle physics.

Over the last decade, xenon TPCs have emerged as powerful tools for the study of rare events, in particular concerning dark matter and neutrinoless double decay ($\beta\beta 0\nu$) searches. Their principle of operation is the same as for all TPCs. Charged radiation ionizes the fluid and the ionization electrons are drifted under the action of an electric field to sensitive image planes, where their transverse position information X,Y is collected. Their arrival times (relative to the start-of-the-event time, or t_0) are then traded to longitudinal positions, Z, through their average drift velocity. Yet, the application of TPCs to $\beta\beta 0\nu$ searches has its own peculiarities. In this case xenon is not only the sensitive medium, but also the target where the decays occur. Since the sensitivity of the search is proportional to the target mass the apparatus needs to be as large and compact as possible, leading to either high pressure xenon (HPXe) or liquid xenon (LXe) TPCs. Furthermore, the energy regime is relatively low (the end-point of the decay $\text{Xe} \rightarrow \text{Ba}^{++} + 2e^-$, $Q_{\beta\beta}$, is 2458 keV) and thus the tracks left by the two electrons can be rather short for HPXe detectors (of the order of 15 cm for electrons with $Q_{\beta\beta}$ energies at 15 bar) or even point-like objects for LXe chambers. Both types of TPCs act as calorimeters, capable of measuring the total energy of the decay and to locate the interaction in a well defined fiducial volume thanks to the availability of a mechanism to signal t_0 , namely the VUV scintillation emitted by xenon as a response to ionizing radiation. In addition a HPXe TPC provides a *topological signature*, thanks to its capability to image the electron tracks.

In this review we discuss the fundamentals, state-of-the-art and potential for the next generation of experiments searching for neutrinoless double beta decay processes with high pressure xenon TPCs. A

more general discussion encompassing the various TPCs used for rare event searches can be found in [Gonzalez-Diaz et al., 2018].

Neutrinoless double beta decay is a hypothetical, very slow radioactive process in which two neutrons undergo β -decay simultaneously and without the emission of neutrinos, $(Z, A) \rightarrow (Z + 2, A) + 2 e^-$. An unambiguous observation of this process would establish that neutrinos are Majorana particles [Majorana, 1937], identical to their antiparticles and would have deep implications in physics and cosmology [Fukugita and Yanagida, 1986].

The simplest mechanism to mediate such a transition is the virtual exchange of light Majorana neutrinos. Assuming this exchange to be dominant at low energies, the half-life of $\beta\beta 0\nu$ can be written as:

$$(T_{1/2}^{0\nu})^{-1} = G^{0\nu} |M^{0\nu}|^2 m_{\beta\beta}^2; \quad (1)$$

where $G^{0\nu}$ is a phase-space integral for the emission of two electrons, $M^{0\nu}$ is the nuclear matrix element (NME) of the transition, and $m_{\beta\beta}$ is the *effective Majorana mass* of the electron neutrino, defined in terms of the neutrino mass eigenstates (m_i) and the elements of the neutrino mixing matrix [Gómez Cadenas et al., 2012].

Over the last decade, several $\beta\beta 0\nu$ experiments, with masses in the range of few tens to few hundreds of kilograms have pushed the sensitivity to the half-life of $\beta\beta 0\nu$ processes by more than one order of magnitude in three different isotopes. Four of these experiments (GERDA [Agostini et al., 2018], EXO [Albert et al., 2018], KamLAND-Zen [Gando et al., 2016b,a], and CUORE [Alduino et al., 2018]) have recently published the results of their analysis. The best limit on the lifetime of a $\beta\beta 0\nu$ isotope was obtained by KamLAND-Zen [Gando et al., 2016b,a]), corresponding to $T_{1/2}^{0\nu} > 1.07 \times 10^{26}$ yr for the $\beta\beta 0\nu$ decay of ^{136}Xe . The GERDA experiment has recently published a limit $T_{1/2}^{0\nu} > 0.8 \times 10^{26}$ yr for the $\beta\beta 0\nu$ decay of ^{76}Ge .

The target of the “next generation” of xenon-experiment is to improve the sensitivity to $T_{1/2}^{0\nu}$ by roughly one order of magnitude, to some 10^{27} yr, or about 20 meV in $m_{\beta\beta}$. If the neutrino mass hierarchy is inverted (e.g. $\Delta m_{31}^2 < 0$, where $\Delta m_{ij}^2 = m_i^2 - m_j^2$ and $m_i, i = 1, 3$ denotes the mass of the three neutrino mass eigenstates), reaching such a sensitivity on $m_{\beta\beta}$ would result in a discovery if the neutrino is a Majorana particle. Even if Nature has chosen a normal hierarchy ($\Delta m_{31}^2 > 0$) a statistical analysis [Agostini et al., 2017] suggests that the probability of discovery would be rather large, around 50%.

Reaching a sensitivity of 10^{27} yr in the half-life $T_{1/2}^{0\nu}$ will require larger exposures (the product of fiducial mass M and observation time t), and thus larger detectors than those of the current generation. The number of events observed in a detector containing a mass M of a $\beta\beta 0\nu$ decaying isotope of atomic weight W and taking data over a period of time t is related with $T_{1/2}^{0\nu}$ through:

$$T_{1/2}^{0\nu} = \epsilon \log 2 \frac{N_A M t}{W N_{\beta\beta}} \quad (2)$$

where N_A is the Avogadro number and ϵ the detector efficiency. In the absence of background, the observation of a single event would determine the existence of the process and measure the value of $T_{1/2}^{0\nu}$. For example, if $T_{1/2}^{0\nu} = 10^{27}$ year, the observation of 1 event in one year in a detector with 30% efficiency would require a mass of 1 tonne.

In the presence of backgrounds, however, the sensitivity to $T_{1/2}^{0\nu}$ will scale like $1/\sqrt{N}$ (where N is the number of observed events) rather than scaling like $1/N$ as in the case of a background-free experiment. Consequently, the sensitivity to $T_{1/2}^{0\nu}$ improves with \sqrt{Mt} rather than with Mt . Alas, equation 1 dictates that the sensitivity to the physical parameter (the effective neutrino mass $m_{\beta\beta}$) goes with the square root of the half-life, and thus each order of magnitude improvement in the latter brings in only a factor 3 improvement in the former. In an experiment where backgrounds need to be subtracted, on the other hand, one needs two orders of magnitude increase in the exposure Mt to improve one order of magnitude in $T_{1/2}^{0\nu}$. It follows that *the next generation of $\beta\beta 0\nu$ experiments must feature target masses in the tonne-range, while aiming to reduce backgrounds to virtually zero.*

Among all the $\beta\beta$ decay isotopes where $\beta\beta 0\nu$ processes could occur, ^{136}Xe is the cheapest and easiest to obtain. Furthermore, xenon is a noble gas that can be dissolved in liquid scintillator (the approach of KamLAND-Zen) or used to build TPCs. The EXO collaboration has pioneered the LXe technology, while the NEXT program [Gomez-Cadenas, 2018] is leading the development of the HPXe technology.

When compared with the other xenon-based experiments, the HPXe technology has the advantage of very good intrinsic energy resolution, and the availability of a topological signature (the observation of the two electrons characteristic of the $\beta\beta 0\nu$ decay) that permits a very low background count in the region of interest (ROI) near $Q_{\beta\beta}$. The main disadvantages is a relatively lower selection efficiency, of the order of 30%, mostly due to the losses of events that radiate bremsstrahlung photons and to the cost of imposing topological recognition. Although not as compact as LXe TPCs, at sufficiently large pressures (*e.g.* 15 bar) a HPXe of relatively modest size (about 10 m^3 of volume) can host masses in the ton scale. Furthermore, the possibility of tagging the Ba^{++} nuclei produced in the $\beta\beta 0\nu$ decay of xenon opens up the possibility of background free searches for xenon-based TPCs.

This review is organized as follows. Fundamentals are discussed in section 2. A quick historical review of the field is presented in 3. Section 4 is devoted to the NEXT program. In section 5 the AXEL and PANDA-X-III proposals are described. Section 6 describes the on-going efforts in barium tagging in HPXe detectors. An outlook is presented in section 7.

2 FUNDAMENTALS

2.1 Operational parameters of a HPXe TPC: pressure, temperature and density

So far, HPXe detectors have operated at ambient temperature with pressures varying between 5 bar—St.Gotthard TPC [Iqbal et al., 1987]— and 20 bar—NEXT-DBDM prototype [Álvarez et al., 2012a]—. The NEXT-White detector [Monrabal et al., 2018] is currently taking data at 10 bar. In practice, at standard temperature, the operational pressure for ton-scale detectors will be in the range 10 bar to 20 bar. Given the density of xenon gas at a pressure of 1 bar and 300 K temperature (5.761 kg m^{-3}), a HPXe TPC of 10 m^3 operating at 10 bar would hold a target mass of near 600 kg (1.2 ton at 20 bar). The detector dimensions, while large (*e.g.* 3.2 m length by 3 m diameter) appear as technically feasible. On the other hand, the NEXT demonstrators (NEXT-DEMO, NEXT-DBDM and NEXT-White) have shown excellent energy resolution and a powerful topological signature in this pressure range.

However, pressure can be traded with temperature, as illustrated in figure 1, which shows the four isochoric (constant density) curves corresponding to pressures of 5, 10, 15 and 20 bar (at a temperature of 20°C). An interesting possibility would be cooling the detector to temperatures near the liquefaction

point (e.g. -70 °C for a density of 0.057 g cm $^{-3}$). The advantages of operating at low temperatures will be discussed in section 4.

2.2 Ionization

When a charged particle propagates through a noble gas, the Coulomb interaction with the atoms results in *ionization* of the medium, releasing on average \bar{n}_e electron-ion pairs, and N_{ex} excited atoms. Sub-excitation electrons, (e.g. free electrons with a kinetic energy lower than the energy of the first excited level), are also produced. This can be expressed as [Aprile and Doke, 2010]:

$$E = N_i E_i + N_{ex} E_{ex} + N_i \epsilon, \quad (3)$$

where E is the energy deposited in the medium in the form of ionization, excitation, and sub-excitation electrons; N_i is the number of electron-ion pairs produced at an average energy deposition E_i , N_{ex} is the number of excited atoms produced at an average energy deposition E_{ex} and ϵ is the average kinetic energy of sub-excitation electrons. Then the expected number of electrons produced for an energy deposition E is:

$$\bar{n}_e = \frac{E}{W_I} \quad (4)$$

where W_I is the average energy required to produce one electron-ion pair. In xenon gas $W_I = 21.9$ eV [Aprile and Doke, 2010]. A $\beta\beta 0\nu$ event of energy 2458 keV results, therefore, in the average production of $112\,337$ electron-ion pairs. In a HPXe TPC a moderate electric field will drift the electrons towards the anode and the ions towards the cathode, minimizing recombination.

2.3 Scintillation

The propagation of a charged particle in a noble gas also results in the emission of VUV scintillation light (with an average wavelength of 172 nm in xenon). Defining W_s as the average energy needed in the creation of one primary scintillation photon, the average number of scintillation photons produced when a particle releases its energy E in the gas is:

$$\bar{n}_\gamma = \frac{E}{W_s} \quad (5)$$

The NEXT collaboration has measured the value of W_s in xenon gas to be [Fernandes et al., 2010]:

$$W_s = 76 \pm 6 \text{ eV} \quad (6)$$

Thus a $\beta\beta 0\nu$ event will release on average $32\,342$ photons. Since light production is isotropic, only a small fraction of the produced photons, Ω , (typically of the order of few %) can be collected. Measurement of the primary scintillation, however, is crucial for a $\beta\beta 0\nu$ detector, as it signals t_0 . A measurement of t_0 is essential to fiducialize the events and remove the large rate of background events that accumulate at the electrodes, and to correct for charge losses occurring during charge drift. Without such corrections, the performance of the detector both in terms of background rate and resolution is seriously compromised.

2.4 Diffusion

As the ionization electrons (and the positive ions) drift towards the anode (cathode) under the action of the electric field, they interact with the noble gas atoms, resulting in both longitudinal and transverse diffusion.

Defining \mathcal{N}_e as the density of electrons per unit volume, $D_{L(T)}$ as the longitudinal (transverse) diffusion coefficient(s), v_d as the drift velocity and η as the attachment coefficient one can write:

$$\mathcal{N}_e(x', y', z', t) = \frac{e^{-\frac{(x'-x)^2+(y'-y)^2}{4D_T(t-t_0)}} e^{-\frac{((z'-z)+v_d(t-t_0))^2}{4D_L(t-t_0)}}}{(4\pi D_T(t-t_0))(4\pi D_L(t-t_0))^{1/2}} \times \bar{n}_e \cdot e^{-\eta v_d(t-t_0)} \quad (7)$$

where the formula applies far from the TPC boundaries [Gonzalez-Diaz et al., 2018]. Here x', y', z' and t denote position and time measured typically at the charge collection plane (the anode), and (x, y, z, t_0) refer to the initial position and time of the ionization cloud, e.g. the interaction point, assumed to be point-like and containing \bar{n}_e electrons. The solution in eq. 7 is an asymmetric gaussian cloud that broadens and losses carriers as it goes on. Arbitrary track topologies can be propagated directly by superposition of such solutions. Choosing $z = 0$ as the coordinate of the amplification plane, and assuming that all charge arrives at a fixed time $t-t_0 \simeq z/v_d$, eq. 7 simplifies to:

$$\mathcal{N}_e(x', y', z') = \frac{e^{-\frac{1}{2}(\frac{x'-x}{D_T^* \sqrt{z}})^2} e^{-\frac{1}{2}(\frac{y'-y}{D_T^* \sqrt{z}})^2} e^{-\frac{1}{2}(\frac{z'}{D_L^* \sqrt{z}})^2}}{(2\pi D_T^{*,2} z)(2\pi D_L^{*,2} z)^{1/2}} \times \bar{n}_e \cdot e^{-\eta z} \quad (8)$$

where $D_{L,T}^* = \sqrt{2D_{L,T}/v_d}$. As it turns out, the electrons produced in a $\beta\beta 0\nu$ decay are extended track in a HPXe detector. One can still make use of eq. 8 making the approximation that the track consists in a superposition of point-like energy depositions that arrive at successive times to the anode.

Diffusion in pure xenon is large, with $D_L^* \sim 10 \text{ mm}/\sqrt{L}$, and $D_T^* \sim 3 \text{ mm}/\sqrt{L}$, where L is the drift length in meters. As a consequence, the ionization electrons produced by tracks located at relatively long distances from the anode will have spread considerably both in the longitudinal and transverse coordinates, and the resulting reconstructed image of the track will be consequently blurred. This undesirable effect can be limited by using mixtures that add a quencher capable of cooling the diffusion electrons and therefore reduce the diffusion.

2.5 Electron lifetime

As primary electrons drift to the anode some of them will be absorbed by impurities in the gas. This results in the so-called “electron lifetime”:

$$\tau_e = (\eta v_d)^{-1} \quad (9)$$

Thus, if the initial number of drift electrons is n_0 (at t_0), the number n reaching the anode at time t will be:

$$n = n_0 e^{-\frac{(t-t_0)}{\tau_e}} = n_0 e^{-\eta z} \quad (10)$$

The main cause of attachment in large TPCs is related to the presence of O_2 . For a given fraction of oxygen concentration, f_{O_2} , the lifetime is inversely proportional to both the square of the pressure, P and f_{O_2} , $\tau_e \propto \frac{1}{P^2} \frac{1}{f_{O_2}}$. The only realistic way to achieve the necessary purity levels is through material selection and continuous recirculation and purification, to minimize the factor f_{O_2} . The dependence with $1/P^2$ is also a major constraint for the operational pressure. In pure xenon the drift velocity is $1 \text{ mm } \mu\text{s}^{-1}$, and thus 1 ms is required to drift 1 m. The drift length of a next-generation HPXe detector with a mass in the ton scale will be in the range 1 m to 3 m. An electron lifetime in the range 10 ms to 30 ms would translate in a 10% charge loss at the maximum drift length. This energy loss can be computed event by event, if t_0 is known, and therefore a correction can be applied, with a residual relative error in the energy equal to the relative error in the determination of the lifetime. Thus, a relative error of 5% in the determination of the lifetime would translate into a residual of 0.5%, which is of the same order of the practical intrinsic resolution in an electroluminescent HPXe TPC (see section 4). Thus, long lifetimes and precise lifetime corrections (which imply a measurement of t_0) are a must for a HPXe TPC aiming for the best energy resolution. Without t_0 the fluctuations in energy introduced by attachment at the large drift distances become very large.

2.6 Intrinsic energy resolution in xenon

Excellent energy resolution is a crucial ingredient for a $\beta\beta 0\nu$ experiment. Indeed, physics allows such resolution to be attained in a gaseous xenon TPC. Instead, those very same physics processes limit the resolution in a liquid xenon TPC. This is clearly seen in figure 2, reproduced from [Bolotnikov and Ramsey, 1997]. The resolutions displayed were extracted from the photo-conversion peak of the 662 keV gamma ray from the ^{137}Cs isotope. Only the ionization signal was detected. A striking feature in figure 2 is the apparent transition at density $\rho_t \sim 0.55 \text{ g/cm}^3$. Below this density, the energy resolution is approximately constant:

$$\delta E/E = 6 \times 10^{-3} \text{ FWHM}. \quad (11)$$

For densities greater than ρ_t , energy resolution deteriorates rapidly, approaching a plateau at LXe density.

The most plausible explanation underlying this strange behavior is the appearance, as density increases, of two-phase xenon ([Nygren, 2007] and references therein). In contrast, given the xenon critical density, the intrinsic resolution in the gas phase is very good up to pressures in the vicinity of 50 bar. Extrapolating the observed relative resolution in figure 2 as $1/\sqrt{E}$ to the ^{136}Xe Q-value ($Q_{\beta\beta}$), allows to predict the intrinsic energy resolution in xenon gas at the region of interest for $\beta\beta 0\nu$ searches, to be $\delta E/E = 3 \times 10^{-3}$ FWHM.

Based on ionization signals only, the above energy resolution reflects an order of magnitude improvement relative to liquid xenon. For densities less than ρ_t , the measured energy resolution in figure 2 matches the prediction based on Fano's theory [Fano, 1947]. The Fano factor F reflects a constraint, for a fixed energy deposited, on the fluctuations of energy partition between excitation and the ionization yield N_I . For electrons depositing a fixed energy E , the rms fluctuations σ_I in the total number of free electrons N_I can be expressed as $\sigma_I = \sqrt{F N_I}$. For pure gaseous xenon (GXe) various measurements [Nygren, 2007] show that $F_{\text{GXe}} = 0.15 \pm 0.02$. In liquid xenon (LXe), however, the anomalously large fluctuations in the partitioning of energy to ionization produce an anomalous Fano factor of $F_{\text{LXe}} \sim 20$, larger than the one corresponding to xenon gas by about two orders of magnitude.

2.7 Electroluminescence

2.7.1 The Gas Proportional Scintillation Chamber

The principle of a Gas Proportional Scintillation Chamber (GPSC) is the following [Conde and Policarpo, 1967]. An X-ray enters through the chamber window and is absorbed in a region of weak electric field ($> 0.8 \text{ kV cm}^{-1} \text{ bar}^{-1}$) known as the drift region. The ionization electrons drift under such field to a region of moderately high electric field (around $3 \text{ kV cm}^{-1} \text{ bar}^{-1}$), the so-called scintillation or EL region. There, each electron is accelerated so that it excites, but does not ionize, the gas atoms/molecules. The excited atoms decay, emitting UV light (the so-called secondary scintillation), which is detected by photosensors. The intensity of the secondary scintillation light is at least two orders of magnitude stronger than that of the primary scintillation. However, since the secondary scintillation is produced while the electrons drift, its latency is much longer than that for the primary scintillation, and its rise time is much longer (up to hundreds of μs for $\beta\beta 0\nu$ events, compared to a few ns). For properly chosen electric field strengths and EL region spatial widths, the number n_{ph} of secondary scintillation photons produced by a single primary electron is nearly constant and can reach values of the order of thousand photons per electron. The average total number, N_t , of secondary scintillation photons produced by an interaction is then $N_t = n_{ph} \cdot N_I$, (recall that N_I is the number of primary ionization electrons) so the photosensor signal amplitude is nearly proportional to E , hence the name of gas proportional scintillation counter (GPSC) for this device.

What made GPSCs extraordinarily attractive was their improved energy resolution compared with conventional Proportional Chambers (PC). In a PC the primary electrons are made to drift towards a strong electric field region, usually in the vicinity of a small diameter (typically $25 \mu\text{m}$) anode wire. In this region, electrons engage in ionizing collisions that lead to an avalanche with an average multiplication gain M of the order of 10^3 to 10^4 . If M is not too large, space charge effects can be neglected, and the average number of electrons at the end of the avalanche, $N_a = M \cdot N_I$, is also proportional to the energy E of the absorbed radiation (hence the name proportional (ionization) counter given to this device). However, for PC detectors, there are fluctuations not only in N_I but also in M ; for GPSCs, since the gain is achieved through a scintillation process with almost no fluctuations, only fluctuations in N_I and in the photosensor need to be considered. Thus, a better energy resolution can be achieved in the latter case.

2.7.2 Electroluminescent yield

A detailed Monte Carlo study of the energy resolution that can be achieved in a high pressure xenon TPC with electroluminescent amplification (HPXe-EL TPC) as a function of the EL yield was performed in [Oliveira et al., 2011]. The study obtained a formula for the the reduced electroluminescence yield, $\left(\frac{Y}{p}\right)$, as a function of the reduced electric field, $\left(\frac{E}{p}\right)$.

$$\left(\frac{Y}{p}\right) = (130 \pm 1) \left(\frac{E}{p}\right) - (80 \pm 3) [\text{photons electron}^{-1} \text{ cm}^{-1} \text{ bar}^{-1}] \quad (12)$$

where the reduced electroluminescence yield is defined as the number of photons emitted per primary electron and per unit of drift length divided by the pressure of the gas, and E/p is expressed in $\text{kVcm}^{-1}\text{bar}^{-1}$. The formula was found to be in good agreement with experimental data measured at 1 bar [Monteiro and others., 2007].

$$\left(\frac{Y}{p}\right) = 140 \left(\frac{E}{p}\right) - 116 [\text{photons electron}^{-1} \text{ cm}^{-1} \text{ bar}^{-1}] \quad (13)$$

2.7.3 Energy resolution in an EL TPC

One of the desirable features of a HPXe-EL TPC is its excellent intrinsic energy resolution, due to the small value of the Fano factor in gaseous xenon and the small fluctuations of the EL yield. Following [Oliveira et al., 2011], the resolution R_E (FWHM) of a HPXe-EL TPC can be written as:

$$R_E = 2\sqrt{2\log 2} \sqrt{\frac{\sigma_e^2}{\bar{N}_e^2} + \frac{1}{\bar{N}_e} \left(\frac{\sigma_{EL}^2}{\bar{N}_{EL}^2}\right) + \frac{\sigma_{ep}^2}{\bar{N}_{ep}^2} + \frac{1}{\bar{N}_{ep}} \left(\frac{\sigma_q}{G_q}\right)^2} \quad (14)$$

In equation 14 the factor $2\sqrt{2\ln 2}$ corresponds to the relation between the FWHM and the standard deviation σ , of a given probability distribution ($\text{FWHM} = 2\sqrt{2\ln 2}\sigma \sim 2.35\sigma$). The first term of the expression is related to fluctuations in the number of primary charges created per event, N_e , the second to fluctuations in the number of EL photons produced per primary electron, N_{EL} , the third reflects the variations in the number of photoelectrons extracted to the photosensor (e.g. PMTs, SiPMs) per decay, N_{ep} , and the fourth the distribution in the photosensor single electron pulse height, G_q .

The primary charge fluctuations are described by the Fano factor, $F = \sigma_e^2/\bar{N}_e$. The fluctuations associated with the electroluminescence production are described by the parameter J defined as the relative variance in the number of emitted VUV photons per primary electron, $J = \sigma_{EL}^2/\bar{N}_{EL}$. The conversion of VUV photons into photoelectrons follows a Poisson distribution, and thus $\sigma_{ep}^2 = \bar{N}_{ep}$. For PMTs, the fluctuations in the photoelectron multiplication gain can be described by $(\frac{\sigma_q}{G_q})^2 = 1$ [Oliveira et al., 2011]. Taking into account the previous relation equation 14 can be rewritten as:

$$R_E = 2.35 \sqrt{\frac{F}{\bar{N}_e} + \frac{1}{\bar{N}_e} \left(\frac{J}{\bar{N}_{EL}}\right) + \frac{2}{\bar{N}_{ep}}} \quad (15)$$

The first term in equation 15, $R(\text{Fano})$, correspond to the intrinsic resolution in xenon, the second term, $R(EL)$ to the resolution associated to fluctuations in electroluminescence and the third, $R(EP)$ to fluctuations in the number of photoelectrons produced in the photosensor plane per $\beta\beta 0\nu$ decay, \bar{N}_{ep} , which can be obtained as:

$$\bar{N}_{ep} = k \bar{N}_e \bar{N}_{EL}, \quad (16)$$

where k is the fraction of EL photons produced per $\beta\beta 0\nu$ decay that gives rise to the production of a photoelectron.

Figure 3 shows the EL yield and energy resolution, R_E as a function of the reduced electric field of a HPXe-EL TPC operating at 15 bar for the energy corresponding to $Q_{\beta\beta}(2458 \text{ keV})$. The values of the EL width (relevant for the yield) and of k (relevant for the resolution) correspond to those of the NEXT-100 detector. Notice that $R(\text{Fano})$ is constant, $R(EL)$ is essentially negligible and $R(EP)$ improves quickly with the reduced field E/P . A typical value of operation for E/P is such that $R(\text{Fano}) = R(EL)$ ($E/P \sim 2$). The combined resolution at this value is around 0.5% FWHM and the yield around 500 photons per electron. Increasing E/P results in very little resolution improvement.

2.8 Avalanche multiplication in HPXe applied to $\beta\beta 0\nu$ searches

The use of avalanche multiplication in HPXe detectors searching for $\beta\beta 0\nu$ processes finds two distinct problems. First, the fluctuation in the gain, G , is considerably larger than F in gas proportional counters involving avalanche multiplication, and thus becomes the dominant term in the resolution. Second, electron multiplication in pure xenon is difficult, due to the fact that VUV scintillation light, copiously produced with the multiplication process, ejects electron from metallic surfaces defining the electrodes. Those electrons, in turn, ionize the gas to the point of breakdown.

The use of quenchers, on the other hand, suppresses the primary scintillation light and has a heavy cost in terms of energy resolution and particle identification (without primary scintillation is not possible to define t_0). Two ways have been considered to solve this problem: a) the use of a “magic gas”, capable to absorb the VUV light emitted by xenon and re-emit it at a more manageable wavelength (*e.g.* in the visible region), without introducing extra fluctuations, and b) the use of micro-pattern devices, such as Micromegas or GEMs whose confined geometrical structure makes them capable, a priori to operate at high pressure without quenchers.

This second possibility was explored in [Balan et al., 2011]. While Micromegas were found, indeed, robust enough to allow operation in pure xenon and at high pressures, their resolution was measured to degrade with increased pressure. It was found that the resolution attainable at $Q_{\beta\beta}$ by micro-bulk micromegas at 10 bar would be 3%, to be compared with that of 0.4% found in [Fernandes et al., 2010] using electroluminescence. Both measurements were carried out with very small setups, in close-to-ideal conditions, and therefore can be taken as reflecting the intrinsic performance of the devices under study.

No magic gas has been found so far capable to re-emit xenon scintillation light at longer wavelengths. Penning mixtures have been tried as a part of the R&D of the NEXT collaboration, as will be further described in section 4.

2.9 Topological signature

Another major advantage of gas relative to liquid—and in general relative to high density calorimeters—is the ability to exploit the topological signal of a $\beta\beta 0\nu$ event, that is the capability to image the tracks left in the gas by the two electrons produced in the $\beta\beta 0\nu$ decay. At 15 bar the track length of the electrons is of the order of 15 cm and can be easily reconstructed in a HPXe TPC. Such a topological signature is not available in LXe detectors, due to the high density of the liquid phase—in fact most other experimental techniques are based in high density calorimeters, none of which can reconstruct the electrons trajectory—.

An electron propagating in high density xenon ionizes the medium and results in a random trajectory due to large multiple scattering. Delta rays and bremsstrahlung photons are emitted along the trajectory. This is shown in figure 4. Even with a detector capable of reconstructing perfectly the electron trajectory, the track would still be wiggled and diffuse due to multiple scattering and the emission of delta rays and photons. Diffusion will further blur the “electron picture”.

There are some differences between a background electron with energy near $Q_{\beta\beta}$ and a “double electron” event emitted by a $\beta\beta 0\nu$ decay where the $Q_{\beta\beta}$ energy is shared between the two electrons. Naively one could expect to be able to distinguish the emission vertex, but this is not possible due to multiple scattering. Other expected features are: a) less “satellite photons” (*e.g.* photons deposited in the chamber and not associated to the electron track) for signal than for background, due to the fact that the background electron has in average twice the energy of the signal electrons and radiates considerably more. Also, the initial trajectory of the background electron is less twisty than that of the double electrons, since

multiple scattering is inversely proportional to the momentum. However, the more powerful “smoking gun” separating signal for background is the energy deposited at the end of the electron trajectory. Near the end of the ionization path (Bragg peak) the electrons deposit suddenly their remaining energy. One can define the end-of-the-track blobs by two spheres of some suitable radius (typically of about 1 cm) around the end-points of the tracks. The energy contained in those spheres is the “blob energy”. The energy of the lowest energy blob of single electrons originated in the gas by photoelectric or Compton interactions of gammas with energies close to $Q_{\beta\beta}$ is much smaller than the energy of the highest energy blob. Instead, the energy of the two blobs is similar for electrons produced in double-electrons produced in a $\beta\beta 0\nu$ decay.

Plotting the energy of each blob reveals a clear separation between signal and background event. The left panel of figure 5 shows the case for background electrons, while the right plot shows the case for signal. In the first case the energy of the lower energy blob is much smaller than the energy of the higher energy blob, in the second case both are roughly the same. A cut requiring that the energy of both blobs is larger than about 250 keV separates very effectively single and double electrons.

3 THE DEVELOPMENT OF THE HPXE AND HPXE-EL TECHNOLOGY FOR $\beta\beta 0\nu$ SEARCHES

The first proposal to search for $\beta\beta 0\nu$ decays using ^{136}Xe was published in 1976 [De’Munari and Mambriani, 1976] (an even earlier paper, by the same authors dates back to 1961 [De’Munari and Mambriani, 1961]). The proposed technology was a self-triggered cloud chamber filled with a mixture of xenon and helium, with helium being the permanent gas of the chamber and xenon acting as condensable vapor. Electroluminescence was proposed to trigger the chamber and to measure the energy of the particles. The setup included an electric field (to produce electroluminescence and clear the ionization) and a magnetic field whose role was to turn the tracks, and thus separate single electrons arising from backgrounds from double electrons arising from $\beta\beta$ decays. Thus, remarkably, two of the major assets of the HPXe-EL technology (*e.g.* energy resolution thanks to proportional amplification of the ionization signal and a topological signature to distinguish two electrons from backgrounds) were identified in this pioneer work.

The concept of gas proportional scintillation counter (GPSC), discussed in section 2.7.1 dates from 1967 [Conde and Policarpo, 1967]. In 1975 the notion of GPSC was combined with that of a TPC, resulting in the Scintillation Drift Chamber (SDC) [Charpak et al., 1975]. A proposal to build a HPXe-EL TPC was made in 1983 [Barabash et al., 1983] (see also [Barabash et al., 1991]). A large SDC with 19 PMTs [Bolzdynya et al., 1997] demonstrated excellent energy resolution at high pressure (9 bar) for high energy X-rays, consistently extrapolating to 0.5% FWHM at $Q_{\beta\beta}$.

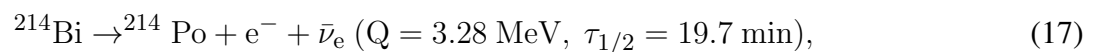
And yet, the early attempts to search for $\beta\beta 0\nu$ processes with high pressure xenon chambers were not based in electroluminescence. The first such attempt was a small ionization chamber (with a mass of 627 g) operating at a pressure of 3 MPa (30 bar) built at the Baksan neutrino observatory [Barabash et al., 1986]. The resolution achieved by this early apparatus (2.7% FWHM at $Q_{\beta\beta}$) was, in fact, better than that attained by subsequent detectors based in multiplication gain. The setup, however, had large ^{222}Rn contamination, due to radon emanating from the purification getters. The Baksan experiment managed to set a first limit of 5.5×10^{19} yr in the lifetime of the $\beta\beta 0\nu$ decay for ^{136}Xe .

At about the same time, a multi-element proportional chamber, operating at 10 bar and with a mass of around 4 kg was built by Fiorini and collaborators —the so-called “Milano experiment”— [Alessandrello et al., 1989]. The resolution achieved was 4.2% FWHM at $Q_{\beta\beta}$. The setup was operated at the LNGS laboratory with natural xenon and with xenon enriched at 64% in the isotope ^{136}Xe . The detector was able

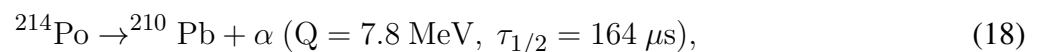
to perform a crude reconstruction of the event topology that allowed the separation between “single cluster events” (*e.g.* single or double electrons with no satellite energy depositions) and “multiple cluster events” (*e.g.* background events where additional energy deposition was identified). However the reconstruction could not separate between single and double electrons. The main source of contamination was the steel wires making up the cells as well as the titanium vessel. The background counting rates were $(5.1 \pm 0.3) \times 10^{-3}$ counts/keV/hour for the enriched xenon sample. The best sensitivity achieved was 1.2×10^{22} yr (at 95% CL) in the lifetime of the $\beta\beta 0\nu$ decay for ^{136}Xe [Alessandrello et al., 1986; Bellotti et al., 1989]. The experiment did not observe the $\beta\beta 2\nu$ mode, setting up a limit of 1.6×10^{20} yr at the 95%CL [Bellotti et al., 1989].

The St. Gotthard TPC (SGTPC) was built in 1987 [Iqbal et al., 1987]. It was a 300 L HPXe detector, built with radiopure materials and operating at a pressure of 5 bar in the St. Gotthard Tunnel Underground Laboratory. The experiment used xenon enriched at 62.5% in the isotope ^{136}Xe . Ionization was read by charge amplification in a wire plane and the transverse position was determined by XY strips. Being a TPC, the longitudinal position was determined by the arrival time of the ionization charge.

In order to quench the VUV light, the SGTPC used a mixture that contained 5% of methane. As a consequence the TPC lacked the information about the start-of-the-event (t_0) and could not fiducialize the tracks along the Z coordinate. The lack of t_0 was a major limitation of this pioneer experiment, since one of the most important backgrounds for a HPXe TPC is the decay:



Due to ^{222}Rn contamination, there is a steady-state concentration of ^{214}Bi in the cathode. In a HPXe TPC with t_0 the bismuth decay described in equation 17 can be vetoed by requiring a fiducial cut on Z. In the absence of t_0 this background becomes dominant, although it can be partially vetoed by looking for a delayed coincidence with an alpha particle due to the decay:



The energy resolution of the SGTPC was 6.6% FWHM at $Q_{\beta\beta}$. This was way worse than the intrinsic resolution expected in xenon. The reasons for the degraded performance were the fluctuations in avalanche gain, and the quenching of the scintillation by the gas mixture, which introduced an irreducible additional fluctuation.

A first search for $\beta\beta 0\nu$ events was published in 1991 [Wong et al., 1991], followed by an improved result in 1998 [Luscher et al., 1998]. The total exposure of the experiment was 12 843 h or about 1.5 yr. The experiment set a limit of 4.4×10^{23} yr in the lifetime of the $\beta\beta 0\nu$ decay mode of ^{136}Xe and a limit of 0.72×10^{22} yr in the $\beta\beta 2\nu$ mode.

The SGTPC was the first detector to demonstrate the topological signature available to a (high pressure) gas TPC. A peculiarity of the experimental technique was that the scan of candidates was done visually. The efficiency and rejection power of the procedure was evaluated by mixing Monte Carlo events with real data. A 68% acceptance for double electrons and a rejection power of 96.5% for single electrons was found. This performance is similar to the best results obtained by the NEXT and PANDA-III-X collaborations using deep neural networks, as will be discussed in sections 4 and 5.

The dominant source of background in the SGTPC were electrons emanating from the cathode that could not be rejected due to the lack of t_0 . Still, the background rate at the ROI of the detector was 0.01counts/(keV · kg · y), the lowest among all the $\beta\beta 0\nu$ searches of the time.

The original proposal for the EXO detector, published in 1999¹ presented a large version of the SGTPC. Like the former, it used multiplication gain to read the ionization, substituting the wire-pad arrangement by micro-pattern structures (GEMs). Operation at a pressure of 5 bar was assumed. PMTs placed in the barrel region were used to read the primary scintillation and thus measure t_0 . In addition, a system of lasers to tag the Ba^{++} ion produced in the $\beta\beta 0\nu$ decay of ^{136}Xe *on the fly*, was envisioned.

The EXO design assumed that the xenon would be mixed with another gas capable of quenching the xenon VUV light (so that the detector could be operated in the regime of charge multiplication without breaking the gas) and at the same time capable of neutralizing one of the positive charges of the Ba^{++} ion, so that tagging based in laser-induced resonance excitation of Ba^+ could be used. At the same time, this gas should be able to cool the drifting electrons, reducing diffusion and re-emit in the visible region, so that t_0 could be measured. Alas, such a “magic gas” was not found neither by EXO, nor by an extensive R&D conducted later by NEXT (see section 4).

To summarize, the GPSC was invented in 1965 and electroluminescence was proposed as early as 1975 for a $\beta\beta 0\nu$ detector. However, the Baksan, Milano and St. Gotthard experiments were all based in electron multiplication for the readout of the ionization. None of these experiments had good energy resolution, but the St. Gotthard TPC demonstrated a powerful topological signature and achieved a very good background rate in the ROI (for the time), in spite of the lack of t_0 which was responsible for most of its background rate. The original EXO proposal also considered avalanche gain as the choice option and later switched to liquid xenon.

The possibility of using a HPXe-EL TPC for $\beta\beta 0\nu$ searches was resurrected in 2009 [Nygren, 2009], and adopted as the baseline solution by the NEXT collaboration in its Letter of Intent [Granena et al., 2009]. The choice of an asymmetric HPXe-EL TPC with an energy plane based in PMTs for energy measurement and a tracking plane based in SiPMs for tracking was established in the NEXT conceptual design report [Álvarez et al., 2011] and further developed in the technical design report (TDR) [Álvarez et al., 2012b]

4 THE NEXT PROGRAM

The Neutrino Experiment with a Xenon TPC (NEXT) is an experimental program developing the technology of high-pressure xenon gas Time Projection Chambers (TPCs) with electroluminescent amplification for neutrinoless double beta decay searches ($\beta\beta 0\nu$).

The first phase of the program included the construction, commissioning and operation of two prototypes, called NEXT-DBDM and NEXT-DEMO (with masses around 1 kg). The NEXT-White² detector, holding 5 kg of xenon implements the second phase of the program. NEXT-White has been running successfully since October 2016 at Laboratorio Subterráneo de Canfranc (LSC), Spain.

NEXT-100 constitutes the third phase of the program. It is a radiopure detector deploying 100 kg of xenon at 15 bar and scaling up NEXT-White by slightly more than 2:1 in longitudinal dimensions. In addition of a physics potential competitive with the best current experiments in the field, NEXT-100 can be

¹ available online at https://www-project.slac.stanford.edu/exo/docs/white_v5.pdf

² Named after the late Prof. James White, a pioneer of the technique and a crucial scientist for the experiment.

considered as a large scale demonstrator of the suitability of the HPXe-EL technology for detector masses in the ton-scale.

The fourth envisioned phase of the program is called NEXT-2.0, a detector that would multiply the mass of NEXT-100 by a factor 5 while at the same time reducing NEXT-100 background in the ROI by at least one order of magnitude, thanks to the combination of an improved topological signature and a reduced radioactive budget. Furthermore, NEXT-2.0 could implement Ba⁺⁺-tagging based in single molecule fluorescence imaging (SMFI) (see section 6). The importance of SMFI Ba⁺⁺-tagging cannot be overemphasized, since it would permit a **background free experiment at the ton scale** leading to a full exploration of the Inverse Hierarchy (IH) and beyond, with a high probability of a discovery.

4.1 The DEMO and DBDM prototypes

The NEXT prototypes were the first HPXe-EL chambers built since the pioneer St. Gotthard TPC experiment discussed in section 3. NEXT-DBDM was instrumented with a single energy plane made of an array of 19 Hamamatsu R7378A 1" photomultipliers capable to operate up to 20 bar pressure. The detector geometry was designed to minimize the dependence of light collection with position. Without a light sensor array near the EL region precise tracking information was not available and only coarse average position could be obtained using the PMT array light pattern. That was sufficient, nonetheless, to fiducialize events within regions of the TPC with uniform light collection efficiencies.

Figure 6 shows the most important result obtained with DBDM. The energy resolution was measured with xenon X-rays and with a radioactive ¹³⁷Cs source, at pressures of 10 and 15 bar. The results obtained approached the intrinsic resolution that could be achieved in xenon (see discussion in section 2.7.3), extrapolating to 0.5% FWHM at $Q_{\beta\beta}^3$.

NEXT-DEMO was a larger-scale prototype of NEXT-100. The pressure vessel had a length of 60 cm and a diameter of 30 cm. The vessel could withstand a pressure of up to 15 bar but was normally operated at 10 bar. The energy plane was instrumented with 19 Hamamatsu R7378A PMTs (same model than DBDM) and a tracking plane made of 256 Hamamatsu silicon photomultipliers (SiPMs). The detector operated for several years demonstrating: excellent operational stability, with no leaks and very few sparks; (b) good energy resolution ; (c) electron reconstruction using the SiPM tracking plane; (d) excellent electron drift lifetime, of the order of 10 ms [Álvarez et al., 2013a,b,c, 2012a; Lorca et al., 2014].

Figure 7 shows the first demonstration of topological signature in an HPXe-EL TPC. The left panel corresponds to single electrons due to photoelectric interactions of the 511 keV gamma emitted in ²²Na decays. The right panel corresponds to tracks selected in the double escape peak of ²⁰⁸Tl and thus it is enriched in "double electrons" (pairs electron-positron). The plots show clearly the difference between "electrons-like" and "double-electrons like" events, which can be easily separated with a cut on the energy of the lower-energy blob as extensively discussed in [Ferrario et al., 2016].

4.2 The NEXT-White detector

The NEXT-White apparatus [Monrabal et al., 2018], shown in figure 8, has roughly the same dimensions as the St. Gotthard TPC experiment, and is currently the world's largest HPXe-EL TPC. The detector operates inside a pressure vessel fabricated with a radiopure titanium alloy, 316Ti. The pressure vessel sits on a seismic table and is surrounded by a lead shield (the lead castle). Since a long electron lifetime is

³ For all energy extrapolations in this report we use, unless otherwise stated, the simple statistical $1/\sqrt{E}$ dependence.

a must, the xenon circulates and is purified in a gas system described in great detail in [Monrabal et al., 2018]. The whole setup sits on top of a tramex platform elevated over the ground at Hall-A, in the LSC.

The right panel of figure 8 shows a selection of the main subsystems of NEXT-White. The TPC is, in essence, a scaled-down version (2:1) of the NEXT-100 TPC, and its construction and operation has been essential to guide the design of the latter. It has a length of 664.5 mm and a diameter of 454 mm. The field cage body is a High Density Polyethylene (HDPE) cylindrical shell of 21 mm thickness. The inner part of the field cage body is machined to produce grooves where radiopure copper rings are inserted (figure 8-a). The drift field is created by applying a voltage difference between the cathode and the gate, through high voltage feedthroughs (figure 8-c). The field transports ionization electrons to the anode where they are amplified. The drift length is (530.3 ± 2.0) mm, and the drift voltage is 400 V cm^{-1} .

The amplification or electroluminescent region is the most delicate part of the detector, given the requirements for a high and yet very uniform electric field. The anode is defined by a Poly-Ethylenedioxythiophene (PEDOT) surface coated over a fused silica plate of 522 mm diameter and 3 mm thickness (figure 8-b). The entire region is mounted on top of the tracking plane to ensure its flatness and is only connected to the rest of the field cage when closing the detector. A thin layer of Tetraphenyl Butadiene (TPB), commonly used in noble gases detectors to shift VUV light to the visible spectrum is vacuum-deposited on top of the PEDOT. The EL gap is 6 mm wide.

The measurement of the event energy as well as the detection of the primary scintillation signal that determines the t_0 of the event is performed by the NEXT-White energy plane (EP), shown in figure 8-d. The Hamamatsu R11410-10 PMTs (figure 8-e) are chosen for their low radioactivity ($(0.37 \pm 0.08) \text{ mBq unit}^{-1}$ in ^{214}Bi) [Cebrián et al., 2017] and good performance. Since they cannot withstand high pressure they are protected from the main gas volume by a radiopure copper plate, 120 mm thick, which also acts as a shielding against external radiation. The PMTs are coupled to the xenon gas volume through 12 sapphire windows welded to a radiopure copper frame that seals against the copper plate. The windows are coated with PEDOT in order to define a ground while at the same time avoiding sharp electric field components near the PMT windows. A thin layer of TPB is vacuum-deposited on top of the PEDOT.

The tracking function in NEXT-White is performed by a plane holding a sparse matrix of SiPMs. The sensors have a size of 1 mm and are placed at a pitch of 10 mm. The tracking plane is placed 2 mm behind the end of the quartz plate that defines the anode with a total distance to the center of the EL region of 8 mm. The sensors are SensL C series model MicroFC-10035-SMT-GP with $35 \mu\text{m}$ cell size and a dark count of less than 100 kHz at room temperature. The cell's size is sufficient to guarantee good linearity and to avoid saturation in the expected operating regime ($\sim 250 \text{ pes } \mu\text{s}^{-1}$). The SiPMs are distributed in 28 boards (DICE boards) with 8×8 pixels each for a total of 1792 sensors (figure 8-g). The DICE boards are mounted on a 120 mm thick copper plate intended to shield against external radiation. The material used for the DICE boards is a low-radioactivity kapton printed circuit with a flexible pigtail that passes through the copper where it is connected to another kapton cable that brings the signal up to the feed-through. Each DICE has a temperature sensor to monitor the temperature of the gas and SiPMs and also a blue LED to allow calibration of the PMTs at the opposite end of the detector. The NEXT-White tracking plane (figure 8-f) is currently the only large system deploying SiPMs as light pixels in the world.

The detector operated with normal xenon during 7 months in 2017 at a pressure of 7 bar (Run II), and during 9 months in 2018 at a pressure of 10 bar (Run IV). Run V, with enriched xenon will start in early 2019. Operation in Run II established a procedure to calibrate the detector with krypton decays

[Martínez-Lema et al., 2018], and provided initial measurements of energy resolution, [Renner et al., 2018], electron drift parameters such as drift velocity, transversal and longitudinal diffusion [Simón et al., 2018] and a measurement of the impact of ^{222}Rn in the radioactive budget, that was found to be small [Novella et al., 2018]. In addition, the performance of the topological signal was measured from the data themselves. Figure 9 shows a selection of preliminary results, including: resolution obtained at high energy fitting the ^{208}Tl photopeak, which extrapolates to 0.85% FWHM at $Q_{\beta\beta}$ (top-left); rate (in Hz/keV) of background events as a function of energy after 41.5 days of low background run, for three different event selections (top-right); signal efficiency versus background acceptance for the topological signature (bottom-left); fiducial background energy spectra, showing good agreement between data and Monte Carlo (bottom-right).

Run IV has demonstrated excellent operational stability, and a long electron lifetime, which in turn translates in improved resolution. Furthermore, the background rate of the detector has been reduced a factor of 4 with respect to Run II, thanks to operation in a radon-free atmosphere and enhanced external shielding. Preliminary results indicate good agreement between the measured data and the Monte Carlo background model, with an average rate of 2 mHz.

4.3 The NEXT-100 detector

The NEXT-100 apparatus is shown schematically in figure 10. The fiducial region is a cylinder of 1050 mm diameter and 1300 mm length (1.27 m^3 fiducial volume) holding a mass of 97 kg of xenon gas enriched at 90 % in ^{136}Xe , and operating at 15 bar. The energy plane (EP) features 60 PMTs. The tracking plane (TP) features an array of 5600 SiPMs. NEXT-100 is essentially a 2:1 scale up version of NEXT-White.

The combination of excellent energy resolution and background rejection provided by the topological signature results in a very low background rate of 4.5×10^{-4} counts/kg/keV/yr [Martín-Albo et al., 2016]. The projected background in the ROI for NEXT-100 is 0.7 counts/yr, with the leading background sources being the PMTs and the substrates of the SiPMs as illustrated in figure 11. The overall efficiency of the detector is 32%. NEXT-100 is scheduled to start in operations in 2020. NEXT-100 will reach a sensitivity of 1×10^{26} yr in $T_{1/2}^{0\nu}$ after a exposure of 500 kg yr. Although this is the same sensitivity achieved by KamLAND-Zen, the capability of NEXT-100 to provide a nearly background-free experiment at the 100 kg scale, and the potential (discussed below) to improve its radioactive budget, resolution and topological signature so that background-free experiments at the ton scale are also possible, is the strongest asset of the experiment.

4.4 Exploring the inverted hierarchy with NEXT-2.0

As discussed in the introduction, exploring the inverse hierarchy (IH) requires detectors with large masses (in the range of the ton) which should be ideally background free. The detrimental effects of the presence of background are illustrated in figure 12, which shows the sensitivity to $m_{\beta\beta}$ (using a reasonable set of nuclear matrix elements) of a fully efficient ^{136}Xe experiment as a function of exposure, for different background rates. A fiducial exposure of almost 2 t yr (corresponding to an actual exposure of 6 t yr, when accounting for an efficiency of the order of 30%) is required for a full exploration of the inverse hierarchy for 0.1 events of background or less. The exposure increases to 3 t yr (9 t yr) for <1 events of background and degrades rapidly for larger backgrounds.

The HPXe-EL technology can be scaled up to multi-tonne target masses while keeping extremely low levels of background by introducing several new technological advancements [Gomez-Cadenas, 2018], including: a) the replacement of PMTs (which are the leading source of background in NEXT-100) with

SiPMs, which are intrinsically radiopure, resistant to pressure and able to provide better light collection; b) operation of the detector at 175 K, not far from the gas triple point. Operation in this regime has two marked advantages: i) it reduces the dark count rate of the SiPMs by a factor 300 and ii) it permits operation at a lower pressure than NEXT-100 (15 bar at 293 K) for the same gas density, as shown in figure 1. Reducing the pressure, in turn, simplifies the construction of future larger detectors; c) operation of the detector with a low diffusion mixture, for example a 0.85/0.15 xenon/helium mixture [Felkai et al., 2018], which reduces the large transverse diffusion of natural xenon gas from $10 \text{ mm}/\sqrt{m}$ to $2 \text{ mm}/\sqrt{m}$, resulting in sharper reconstructed images for the electron trajectories and improving the performance of the topological signature [Renner et al., 2017] —other possible mixtures have been investigated in [Henriques et al., 2017]—.

The improvement of the topological signature in low diffusion regime is illustrated in figure 13. The left panel shows the three projections of a reconstructed Monte Carlo electron in the case of high diffusion (top display) and low diffusion (bottom display). For the large transverse diffusion of natural xenon ($\sim 10 \text{ mm}/\sqrt{L}$, where L is the length drifted by the electrons), the optimal size of the x, y, z “voxels”, making up the reconstructed track is $10 \times 10 \times 5 \text{ mm}^3$ —for smaller voxels, the large diffusion results in disconnected tracks—. For the smaller transverse diffusion of a 0.85/0.15 xenon/helium mixture, ($\sim 2 \text{ mm}/\sqrt{L}$) the track can then be reconstructed with much smaller voxels, $2 \times 2 \times 2 \text{ mm}^3$. The right panel of figure 13 shows the expected efficiency versus rejection power of the topological cut separating single and double electrons for high diffusion (solid line, large voxels) and low diffusion (dashed line, small voxels). The figure of merit shown in figure maximizes in an efficiency close to 70% in both case, but the background accepted is 6.6% for high diffusion and 2.5% for low diffusion. Thus, a reduction of 2.6 in background is achieved.

The NEXT collaboration is planning a future detector, provisionally called NEXT-2.0, that will incorporate all the above improvements, while deploying masses in the ton scale. If the tantalizing possibility of tagging the Ba^{++} ion is confirmed, NEXT-2.0 could incorporate a Ba^{++} tagging system. The target background of NEXT-2.0 is $<1 \text{ events t}^{-1} \text{ yr}^{-1}$, allowing the experiment to reach a sensitivity of $1 \times 10^{27} \text{ yr}$ in $T_{1/2}^{0\nu}$ with an exposure of 5.0 t yr . This performance would improve the current state of the art by a factor of 10, opening the possibility for a discovery. With Ba^{++} -tagging, NEXT-2.0 would be a truly background free experiment, capable to explore even further (or faster) the physical parameter space. Importantly, all the crucial technology improvements for NEXT-2.0 *can be demonstrated* by suitable upgrades of the NEXT-100 detector, which would permit testing each of the crucial steps leading to the ton-scale technology, namely cool gas operation, SiPM as energy sensors, low diffusion mixtures and barium tagging.

4.5 HXe TPCs based in electron multiplication: the NEXT-MM prototype

Although the baseline of the NEXT program is electroluminescence, a vigorous R&D was conducted to assess the performance and potential of a HPXe TPC based in electron multiplication [Gonzalez-Diaz et al., 2015; Álvarez et al., 2014]. As extensively discussed in this report, the use of avalanche gain to amplify the ionization signal implies a cost in energy resolution with respect to electroluminescence. Such a cost could, in principle, be compensated by other factors.

One of them is radiopurity. Micropattern structures such as micromegas are very light and can be manufactured with radiopure components (*e.g.* copper, kapton), thus offering a very radiopure readout system. Yet, the same applies to readouts based in SiPMs [Cebrián et al., 2015]. Indeed, as discussed above, the main source of internal background in the NEXT-White and NEXT-100 detectors is the PMTs in the energy plane. However, getting rid of the PMTs is not easy, since they are needed to detect primary

scintillation and thus provide a measurement of t_0 . Indeed, the current trend in underground experiments both searching for Dark Matter and for $\beta\beta 0\nu$ decays is replacing the PMTs with SiPMs, mounted on ultra-pure substrates. Such sensor arrangement will likely be as radiopure or more than micro-pattern-based readout planes.

The use of micromegas alone does not provide a way to measure t_0 and therefore one would need to revert to an asymmetric TPC, perhaps considering a detector that uses a plane of SiPMs behind the cathode to read primary scintillation and a micromegas-based readout located in the anode that would provide the event energy and topology. This solution has the same drawback already mentioned when discussing the early EXO proposal. One needs to build a large energy plane anyway, that could measure the energy with far better resolution than the solution being adopted.

A second reason to consider a micro-pattern device readout is the possibility to combine a very fine pitch (*e.g.* finely pixelized micro-bulk micromegas) with a low diffusion gas mixture, in order to improve the topological signature. In order to keep t_0 such a low diffusion mixture also needs to shift the xenon VUV light to the visible or near UV spectrum, since the performance of micromegas in pure xenon deteriorates at high pressure, as discussed in section 2.

In [Gonzalez-Diaz et al., 2015; Álvarez et al., 2014], the NEXT collaboration investigated the possibility that a mixture of xenon with Trimethylamine (TMA) could reduce electron diffusion while simultaneously displaying Penning effect and scintillation. Furthermore TMA could also provide charge neutralization of Ba^{++} to Ba^+ , as needed for some Ba-tagging schemes (see section 6).

The studies were carried out with a medium-size HPXe TPC called NEXT-MM, of dimensions similar to NEXT-DEMO (73 L). The detector was instrumented with a large microbulk-Micromegas readout plane [Álvarez et al., 2014], covering an area of 700 cm^2 and comprising 1152 pixels of $8 \times 8 \text{ mm}^2$.

The main results of those studies, using a mixture containing 2.2% of TMA and operating at 10 bar were:

1. The use of TMA allowed stable operation of the micromegas-based system at high pressure.
2. TMA quenches the primary VUV xenon scintillation light even in very small concentrations. On the other hand, TMA scintillation was observed above 250 nm at the level of 100 photons per MeV in [Nakajima et al., 2015]. In another study [Trindade et al., 2018], TMA scintillation was not observed and a limit on re-emission w.r.t. the primary VUV light of 0.3% was set. The conclusion is that in xenon-TMA mixtures it is not possible to use scintillation to measure t_0 .
3. The use of TMA reduced by a large factor both the longitudinal and transverse diffusion, w.r.t. pure xenon. The measured values of D_L^* at 1 bar ranged between $340 \mu\text{m}/\sqrt{\text{cm}}$ and $649 \mu\text{m}/\sqrt{\text{cm}}$ depending of the value of the reduced electric field, a reduction of 2-3 w.r.t. pure xenon. The measured value of the transverse diffusion was $D_T^* \sim 250 \mu\text{m}/\sqrt{\text{cm}}$, that is a factor 10 w.r.t. pure xenon.
4. The energy resolution (FWHM) ultimately achieved on the full fiducial volume was 14.6% at 30 keV, with contributions from the limited S/N, sampling frequency and non-uniformity of the readout plane explaining the deterioration with respect to results obtained earlier in small setups (9%).
5. The calorimetric response to 511 keV and 1275 keV electron tracks extrapolated to $Q_{\beta\beta}$ gives energy resolutions varying from 3.2% FWHM (for the best sector) to 3.9% FWHM in the full TPC.
6. Due to the very low electron diffusion measured for the mixture (at the scale of 1 mm for 1 m drift), and the easiness at increasing the readout granularity, the technology offers the possibility of mm-accurate true-3D reconstruction of MeV-electron tracks on large detection volumes and at high

pressure. Unfortunately, the lack of a source of double electrons in the system prevented from a full study characterizing the topological signature in this device as those carried out in NEXT-DEMO and NEXT-White.

In conclusion, this R&D confirmed both the advantages —excellent track reconstruction due to reduced diffusion— and disadvantages —worse energy resolution— of using electron amplification, known since the pioneer work of the St. Gotthard TPC. The fact that TMA does not behave as a “magical gas” (its scintillation cannot be used to measure t_0), excludes its use for a future ton-scale experiment, unless alternative ways of measuring t_0 are found.

5 OTHER HPXE PROPOSALS

5.1 AXEL

AXEL is an R&D lead by the U. of Kyoto, in Japan. The envisioned AXEL detector is almost identical to the NEXT design. Both are HPXe-EL TPCs, with an energy plane (AXEL assumes PMTs, as the NEXT-100 detector) and a tracking plane based in SiPMs. In the AXEL concept, however, the SiPMs are VUV sensitive and provide a measurement of the energy of the event in addition of a reconstruction of the topological signal. Rather than an open EL region, AXEL introduces the concept of Electroluminescence Light Collection Cell (ELCC), shown in figure 14. The ELCC consists of an anode plate, a supporting PTFE plate, a mesh and a plane of VUV SiPMs. The anode plate and PTFE have holes aligned with the SiPMs and define a cell structure. By applying high voltage between the anode plate and the mesh, ionized electrons are collected into the cells along the lines of electric field, and generate EL photons, which are detected by the SiPMs cell by cell. Because the EL region is contained in each cell, a measurement of the energy with this arrangement has a milder dependence on event position than in the case of the open grid used by NEXT. Notice, however, that the energy of the event in NEXT is measured with the PMT plane, while in AXEL the same PMT plane is only used to detect the primary scintillation light and thus measure t_0 . This is due to the fact that the ELCC does not produce enough backward-going light, since only the photons moving along the narrow channel defined by the cell escape the structure, while all the others are absorbed.

A small prototype has been developed by the AXEL collaboration. The detector is 6 cm long and has a diameter of 10 cm. The ELCC plane has 64 3×3 Hamamatsu SiPMs arranged in a 8×8 matrix and placed at 7.7 mm pitch. Two VUV sensitive PMTs, capable to operate up to 10 bar pressure provide t_0 . The detector has operated at a pressure of 4 bar and calibrated with low energy X-rays produced by a ^{57}Co source.

The energy resolution was measured using the xenon X-rays [Ban, 2017] (of energies 29.8 keV, 33 keV) as well as the photoelectric and escape peak from the ^{57}Co source (energies of 122 keV, 92 keV). The energy resolution as a function of the peak energy was fitted to the simple statistical model $a\sqrt{E}$ and also to a function of the form $a\sqrt{E + bE^2}$, which described better the data. The extrapolation to $Q_{\beta\beta}$ was 0.85% using the $a\sqrt{E}$ law, and 2.03% using the law with an additional constant term.

Thus, in terms of energy resolution, the ELCC does not appear to bring an improvement over the open grid used by NEXT (notice that the NEXT-White detector measures krypton X-rays, of energy 41.5 keV, with a resolution of $3.86 \pm 0.01\%$ in the central region of the detector, which extrapolates to 0.5% at $Q_{\beta\beta}$, to be compared with 4% obtained by the AXEL prototype for the 122 keV gamma, which extrapolates to 0.9% at $Q_{\beta\beta}$). On the other hand PMTs are still needed to measure t_0 and those PMTs could measure the

energy with better resolution that AXEL has achieved so far. It remains to be seen if the ELCC brings an improvement to the topological signal. So far, the energies investigated by AXEL are too small to produce significant tracks.

On the other hand, the AXEL R&D addresses two important points. One is the need to build very large EL structures for future ton-scale detectors. In that respect, the modular nature of the ELCC appears, a priori, well suited to scale up to large dimensions. The second point is the interest to measure the energy at the anode, if the cathode is to be used, in a future experiment for Ba⁺⁺ tagging. However, the ELCC provides only a partial solution, since AXEL still needs to instrument the cathode with PMTs to measure t_0 . Further progress is to be expected with the planned larger prototype that the AXEL group plans to build in the near future.

5.2 PandaX-III

The PandaX-III collaboration [Chen et al., 2017] has proposed the construction of a detector which is essentially a large-scale version of the NEXT-MM prototype discussed in section 4, that is, a HPXe TPC based in electron amplification with a micromegas-based readout and a xenon-TMA mixture. Their main argument for their technological choice are the reduction of background associated with the PMT energy plane, and the expected enhancement of the topological signature.

The performance of the topological signature expected in the detector has been quantified with Monte Carlo studies. A selection efficiency of 59% for signal with a rejection of the background at the level of 97% is found using a blob-search analysis. The results improve when using deep neural networks, which result in an 80% signal efficiency and 98% background rejection [Han, 2017]. This result is comparable with that obtained by NEXT using low diffusion mixtures (70% signal efficiency, 97.5% background rejection). Indeed, both the PANDAX-III and the NEXT studies using DNNs show that the separation between single and double electrons in dense xenon gas reaches an intrinsic limit where about 2% of the background events fake the signal event for perfect reconstruction. Those are events where multiple scattering or Bremsstrahlung in single, energetic electrons, “fake” an energetic blob at the beginning of the electron track.

The parameters of the first PANDAX-III module are described in [Han, 2017]. The expected energy resolution (3% at $Q_{\beta\beta}$) is consistent with the best results obtained by NEXT-MM. The efficiency (35%) is typical of a HPXe TPC with track reconstruction and also consistent with that found by the NEXT detectors.

Comparing PANDAX-III with the SGTPC, we notice that both detectors are rather similar, in particular concerning the performance of the topological signature, since both operate in the low diffusion regime (recall from section 3 the excellent performance of the topological signal of SGTPC). On the other hand, the energy resolution of the SGTPC was roughly a factor two worse than that projected by PANDAX-III, and none of the two detectors had t_0 , thus one expects similar background level associated with radon degassing at the cathode. Yet, the SGTPC measured a background rate of 10^{-2} counts/(keV · kg · y), which is a factor 100 worse than the projected background level of PANDAX-III (10^{-4} counts/(keV · kg · y)). A naive expectation in terms of energy resolution would be a factor two improvement. This suggests that the background rate estimation of PANDAX-III may be somewhat optimistic.

6 BARIUM TAGGING IN A HPXE TPC

It has long been recognized that the detection of single barium ions emanating from the decay of ^{136}Xe , when combined with a Gaussian energy resolution better than 2% FWHM—needed to reject $\beta\beta 2\nu$ events which also produce barium ion—, could enable a background-free $\beta\beta 0\nu$ experiment, since no conventional radioactive process can produce a barium ion in the gas xenon.

A method to tag barium in a HPXe TPC was proposed in 2000 [Danilov et al., 2000], following the idea pointed out in [Moe, 1991] of using laser induced fluorescence to tag the presence of a Ba^+ ion in xenon gas.

The level structure of the Ba^+ ion shows a strong 493 nm allowed transition, and therefore ground-state ions can be optically excited to the $6^2P_{1/2}$ state from where they have substantial branching ratio (30%) to decay into the metastable $5^4P_{3/2}$ state. A Ba^+ ion confined in a radio frequency trap can then be illuminated with suitable lasers to induce fluorescence. Specific Ba^+ detection is achieved by exciting the system back into the $6^2P_{1/2}$ state with 650 nm radiation and observing the blue photon from the decay to the ground state (70% branching ratio). This transition has a spontaneous lifetime of 8 ns and radiates 6×10^7 photons/s.

While the technique has been established by atomic physicists since 1978 the application of it to a $\beta\beta 0\nu$ experiment in a large HPXe TPC presents many formidable problem. The method proposed in [Danilov et al., 2000] assumed that the ion position in the TPC could be located *in flight* and illuminated with a pair of lasers tuned onto the appropriate frequencies and simultaneously steered to the place where the $\beta\beta 0\nu$ candidate event was found. This is far from easy in a large HPXe TPC as those foreseen for the next-generation of neutrinoless double beta experiment. Additional complications were the detection of the fluorescence and the Doppler broadening of the transition line width at high pressure. Finally, barium resulting from double beta decay is initially highly ionized due to the disruptive departure of the two energetic electrons from the nucleus Green [1957]. Rapid capture of electrons from neutral xenon is expected to reduce this charge state to Ba^{++} , which may then be further neutralized through electron-ion recombination. Unlike in liquid xenon, where recombination is frequent and the barium daughters are distributed across charge states Albert et al. [2015], recombination in the gas phase is minimal Bolotnikov and Ramsey [1997], and thus Ba^{++} is the expected outcome. Thus, an additional transfer gas needs to be added to xenon, capable of transferring Ba^{++} to Ba^+ . TEA has been demonstrated to do the job [Sinclair et al., 2011] and similar gases such as TMA will probably also work. On the other hand, those very same gases quench the scintillation signal and thus the event cannot be located in the longitudinal coordinate. This fact alone makes the prospect for in-situ tagging very dim.

Since 2000, the R&D effort in barium-tagging has branched to two main lines. Tagging in liquid xenon [Mong et al., 2015]—not discussed in this report—, and tagging in high-pressure gas with two main approaches: a) extracting the Ba^{++} ion to a secondary detection volume via funneling, and b) tagging the Ba^{++} ion in a suitable detector located in the cathode.

In fact, both approaches are not incompatible. The key notion proposed in [Brunner et al., 2015] is to develop an RF ion-funnel to extract the Ba^{++} from the high pressure detector. If this is achieved the detection of the ion could proceed via guiding it to a quadrupole trap and using laser induced fluorescence or any other method. In particular, the ion could be guided to a Ba^{++} ion detector. On the other hand, the very same RF-carpets proposed for funneling the ion outside the HPXe can be used to guide it to a small region in the cathode itself, where they can be detected. Both approaches (in-situ versus extraction) have their cons and pros and both need still considerable R&D (much of it synergic) to establish their feasibility.

Yet, tagging “in situ”, without lasers needs of a new detection technique. Such a technique, based in Single Molecule Fluorescence Imaging (SMFI) was proposed in [Nygren, 2014].

SMFI is a technique invented by physicists and developed by biochemists that enables single-molecule sensitive, super-resolution microscopy. Among the applications of SMFI are the sensing of individual ions Lu and Paige [2007], demonstrated in various environments, including inside living cells Stuurman and Vale [2006]. In SMFI, a thin layer containing potentially fluorescent molecules is repeatedly illuminated with a laser at frequencies in the blue or near ultraviolet range. The response of the molecule depends on whether they have captured a specific ion—for example Ca^{++} which is of great interest in neurological applications, given its role as neurotransmitter channel—or not. Chelated molecules (molecules that have captured an ion) fluoresce strongly, while un-chelated (ion-free) molecules respond very weakly. Image-intensified CCD cameras are used to detect single photons and precisely identify and localize single molecules.

The NEXT collaboration is pursuing a program of R&D to tag the barium ion using SMFI techniques. Since the Ba^{++} energy in high pressure gas is thermal, and charge exchange with xenon is highly energetically disfavored, the Ba^{++} state is expected to persist through drift to the anode plane. For this reason, and because barium and calcium are congeners, dyes which have been developed for Ca^{++} sensitivity for biochemistry applications provide a promising path toward barium tagging in HPXe. In [Jones et al., 2016] the properties of two such dyes, Fluo-3 and Fluo-4 were explored. In the presence of Ba^{++} excitation at 488 nm yielded strong emission peaking around 525 nm, demonstrating the potential of these dyes to serve as barium tagging agents.

A convincing proof-of-concept was carried out by the NEXT collaboration in [McDonald et al., 2018]. The experiment managed to resolve individual Ba^{++} ions on a scanning surface using an SMFI-based sensor.

The SMFI sensor concept uses a thin quartz plate with surface-bound fluorescent indicators, continuously illuminated with excitation light and monitored by an EM-CCD camera. It is anticipated that such a sensor would form the basis for a Ba^{++} detection system in HPXe, with ions delivered to a few $\sim 1 \text{ mm}^2$ sensing surfaces, first via drift to the cathode and then transversely by RF-carpet [Arai et al., 2014], a method already demonstrated at large scales [Gehring et al., 2016] and for barium transport in HPXe [Brunner et al., 2015], as discussed above.

To demonstrate single Ba^{++} the proof-of-concept imaged individual near-surface Ba^{++} ions from dilute barium salt solutions using total internal reflection fluorescence (TIRF) microscopy [Burghardt, 2012]. The fluorophores used as detectors were fixed at the sensor surface. This emulates the conditions in a HPXe TPC detector, where the ions will drift to the sensor plate and adhere to fluorophores immobilized there.

The hallmark of single molecule fluorescence is a sudden discrete photo-bleaching transition Habuchi et al. [2005]. This occurs when the fluorophore transitions from a fluorescent to a non-fluorescent state, usually via interaction with reactive oxygen species Thomas et al. [2000]. This discrete transition signifies the presence of a single fluor, rather than a site with multiple fluors contributing. The 375 s scan time is significantly longer than the typical photo-bleaching time of Fluo-3 at this laser power Thomas et al. [2000], so the majority of spots are observed to bleach in our samples. A typical near-surface fluorescence trajectory is shown in figure 15. In summary, the NEXT proof of concept shows that SMFI can be used to resolve individual Ba^{++} ions at surfaces via TIRF microscopy. Ba^{++} ions have been detected above a background of free residual ions at 12.9σ statistical significance, with individual ions spatially resolved and observed to exhibit single-step photo-bleaching trajectories characteristic of single molecules.

An SMFI sensor in a future HPXe TPC will differ from the apparatus described here in a few key ways. First, the fluorophores will be surface-tethered, and not embedded in a thick sample. Thus, only near-surface bright spots are expected, and offline separation from the deeper background fluors will not be necessary. Second, the target signature will be appearance of a new candidate over a pre-characterized background, coincident in a spatio-temporal region with an $\beta\beta 0\nu$ candidate in the TPC. In this case, only the ability to resolve appearance of a new ion is important, and the spatial localization of individual ion candidates demonstrated here shows that many can be recorded on the same sensor before saturation. Third, the micro-environment around the Fluor will be different, being immobilized on a dry surface rather than within a PVA matrix, and this may modify chelation and fluorescence properties of the Fluor. Finally, the extent to which photo-bleaching will be active in a clean HPXe environment is unknown. Thus, there is still a long and uncertain R&D road ahead before barium tagging can be successfully implemented in a HPXe detector searching for $\beta\beta 0\nu$ decays.

7 OUTLOOK

The Time Projection Chamber (TPC), invented by D. Nygren in 1975 revolutionized the imaging of charged particles in gaseous detectors. This article has presented a review of the application of high pressure xenon (HPXe) TPCs to the search for neutrinoless double beta decay ($\beta\beta 0\nu$) processes. This field has been active for more than half a century, but its importance has been re-asserted with the discovery of neutrino oscillations and the implications that neutrinos have mass. Massive neutrinos could be Majorana particles, identical to their own antiparticles, a fact that would be unambiguously proven if $\beta\beta 0\nu$ processes are observed.

The simplest mechanism to mediate $\beta\beta 0\nu$ decays (the exchange of a light neutrino) provides a rationale to evaluate the state-of-the-art and prospects of the field. The current generation of $\beta\beta 0\nu$ experiments have explored half-lives in the vicinity of 10×10^{26} yr, corresponding to effective neutrino masses—in the case of xenon and for the most favorable nuclear matrix element—in the vicinity of 60 meV. The next generation of experiments aims to reach half-lives of at least 10×10^{27} yr and thus explore effective neutrino masses of up to 20 meV, with a significant probability of making a discovery.

To be sensitive to $\beta\beta 0\nu$ half-lives in the range of 10×10^{27} yr and more, it is mandatory that the next-generation experiments deploy exposures in the range of up to 10 ton · yr, and a background rate in the ROI as close to zero as possible. This tremendous challenge all but forces a paradigm shift in the experimental techniques of the field.

High Pressure Xenon TPCs offer one of the most attractive approaches to address such a daunting challenge thanks to the combination of: a) excellent energy resolution; b) the availability of a robust topological signature that allows full fiducialization of the events, identification of satellite clusters (signaling Compton scatters and other background processes) and the capability to separate single (background) from double (signal) electrons. HPXe TPCs can be built with ultra-pure materials and are scalable to large masses. On top of that, the possibility to tag the daughter Ba^{++} ion produced in the decay $\text{Xe} \rightarrow \text{Ba}^{++} + 2e^{-} (+2\nu)$, may provide a way to build truly background-free experiments.

The use of xenon for $\beta\beta 0\nu$ searches was proposed as early as 1961, and the realization that electroluminescence (EL) was a promising way to achieve excellent energy resolution dates from 1975 (as part of the first detector proposal, a bubble chamber), and was revisited in 1983. However, the first generation of HPXe detectors (the Baksan and Milano experiment) did not use EL but electron amplification. The first true HPXe time projection chamber—the St. Gotthard TPC— was also based in avalanche gain,

and used a mixture 0.95-0.05 Xe/CH₄ to stabilize the gas, which quenched the primary scintillation (thus the detector had to make do without t_0) and resulted in mediocre energy resolution ($\sim 7\%$ at $Q_{\beta\beta}$). However, the SGTPC also proved the robust topological signal available to the technology and boasted the lowest background rate level (10^{-2} counts/(keV · kg · y)) of its time.

And yet, after the SGTPC the technology was frozen for two decades, until it was resurrected again by the NEXT experiment, which incorporated D. Nygren's proposal to build an EL TPC, along with technological solutions developed by J. White and one of the authors of this review (JJGC). The NEXT program has built two large prototypes and a detector of the size of the SGTPC (NEXT-White), which is currently taking data at the Canfranc Underground Laboratory and has already shown excellent energy resolution (1% FWHM at $Q_{\beta\beta}$), and a robust topological signal, along with a well understood background model. The NEXT-100 detector, currently in early phase of construction (scheduled to start data taking in 2020), can achieve a sensitivity competitive with the best experiments of the current generation while at the same time demonstrating the potential of the technology for a background free experiment.

Two other projects are proposing HPXe TPCs for $\beta\beta 0\nu$ searches. One is AXEL, in Japan, which has so far developed a small prototype in which the interesting concept of Electroluminescence Light Collection Cell (ELCC) is explored. The other is PANDAX-III, which proposes what is essentially a large-scale version of the SGTPC, using micromegas (rather than wires and pads) for readout, and TMA (rather than CH₄) as quencher. As it was the case with SGTPC, PANDAX-III is expected to feature an excellent topological signature but has the double handicap of a mediocre resolution (3–4 % FWHM according to the R&D measurements done in the context of the NEXT collaboration) and lack of t_0 .

This review has also summarized the state-of-the-art of Ba⁺⁺ tagging in gaseous HPXe detector. R&D has been conducted in this front by the EXO collaboration (which is also studying Ba⁺⁺ tagging in liquid and solid xenon) and by NEXT. The EXO-gas collaboration has studied the possibility to extract the Ba⁺⁺ ion out of the main chamber through funneling, while NEXT is studying the the potential of applying Single Molecular Fluorescence Imaging, SMFI (also proposed by Dave Nygren) to barium tagging with very promising initial results.

In summary it appears that the HPXe technology, in particular using electroluminescence and barium tagging, can assert itself as one of the major possibilities for the next generation of $\beta\beta 0\nu$ experiments.

CONFLICT OF INTEREST STATEMENT

The authors declare that the research was conducted in the absence of any commercial or financial relationships that could be construed as a potential conflict of interest.

FUNDING

This research work has been supported by the European Research Council (ERC) under the Advanced Grant 339787-NEXT the Ministerio de Economía y Competitividad of Spain under grants FIS2014-53371-C04, and the GVA of Spain under grants PROMETEO/2016/120 and SEJI/2017/011.

ACKNOWLEDGMENTS

We gratefully acknowledge the privilege of working and learning from Dave Nygren, and the late James White. We would also like to acknowledge José Ángel Hernando, Michel Sorel, Pau Novella, Joaquim dos

Santos, Lior Arazi and our colleagues of the NEXT collaboration for many fruitful discussions. We also acknowledge Oliviero Cremonesi and Alexander Barabash for their kind input on the historical development of the HPXe technology.

REFERENCES

- Agostini, M., Benato, G., and Detwiler, J. (2017). Discovery probability of next-generation neutrinoless double- β decay experiments. *Phys. Rev. D* 96, 053001. doi:10.1103/PhysRevD.96.053001
- Agostini, M. et al. (2018). Improved Limit on Neutrinoless Double- β Decay of ^{76}Ge from GERDA Phase II. *Phys. Rev. Lett.* 120, 132503. doi:10.1103/PhysRevLett.120.132503
- Albert, J. B. et al. (2015). Measurements of the ion fraction and mobility of alpha- and beta-decay products in liquid xenon using the exo-200 detector. *Phys. Rev. C* 92, 045504. doi:10.1103/PhysRevC.92.045504
- Albert, J. B. et al. (2018). Search for Neutrinoless Double-Beta Decay with the Upgraded EXO-200 Detector. *Phys. Rev. Lett.* 120, 072701. doi:10.1103/PhysRevLett.120.072701
- Alduino, C. et al. (2018). First Results from CUORE: A Search for Lepton Number Violation via $0\nu\beta\beta$ Decay of ^{130}Te . *Phys. Rev. Lett.* 120, 132501. doi:10.1103/PhysRevLett.120.132501
- Alessandrello, A., Bellotti, E., Camin, D., Cremonesi, O., Fiorini, E., Liguori, C., et al. (1986). Multielement Proportional Chamber for ^{136}Xe $\beta\beta$ decay. *Nucl. Instrum. Meth.* A252, 227–233. doi:10.1016/0168-9002(86)91181-2
- Alessandrello, A. et al. (1989). *Nuclear Physics* B21, 209
- Álvarez, V. et al. (2011). The NEXT-100 experiment for neutrinoless double beta decay searches (Conceptual Design Report)
- Álvarez, V. et al. (2012a). Near-Intrinsic Energy Resolution for 30 to 662 keV Gamma Rays in a High Pressure Xenon Electroluminescent TPC. *Nucl. Instrum. Meth.* A708, 101–114. doi:10.1016/j.nima.2012.12.123
- Álvarez, V. et al. (2012b). NEXT-100 Technical Design Report (TDR): Executive Summary. *JINST* 7, T06001. doi:10.1088/1748-0221/7/06/T06001
- Álvarez, V. et al. (2013a). Initial results of NEXT-DEMO, a large-scale prototype of the NEXT-100 experiment. *JINST* 8, P04002. doi:10.1088/1748-0221/8/04/P04002
- Álvarez, V. et al. (2013b). Ionization and scintillation response of high-pressure xenon gas to alpha particles. *JINST* 1305, P05025. doi:10.1088/1748-0221/8/05/P05025
- Álvarez, V. et al. (2013c). Operation and first results of the NEXT-DEMO prototype using a silicon photomultiplier tracking array. *JINST* 8, P09011. doi:10.1088/1748-0221/8/09/P09011
- Álvarez, V. et al. (2014). Characterization of a medium size Xe/TMA TPC instrumented with microbulk Micromegas, using low-energy γ -rays. *JINST* 9, C04015. doi:10.1088/1748-0221/9/04/C04015
- Aprile, E. and Doke, T. (2010). Liquid Xenon Detectors for Particle Physics and Astrophysics. *Rev. Mod. Phys.* 82, 2053–2097. doi:10.1103/RevModPhys.82.2053
- Arai, F. et al. (2014). Investigation of the ion surfing transport method with a circular rf carpet. *International Journal of Mass Spectrometry* 362, 56 – 58. doi:http://dx.doi.org/10.1016/j.ijms.2014.01.005
- Balan, C., Freitas, E. D. C., Papaevangelou, T., Giomataris, I., da Luz, H. N., Monteiro, C. M. B., et al. (2011). Micromegas operation in high pressure xenon: Charge and scintillation readout. *JINST* 6, P02006. doi:10.1088/1748-0221/6/02/P02006
- Ban, S. (2017). AXEL : Neutrinoless double beta decay search with a high pressure xenon gas Time Projection Chamber. *J. Phys. Conf. Ser.* 888, 012233. doi:10.1088/1742-6596/888/1/012233

- Barabash, A. S., Golubev, A. A., Kazachenko, O. V., Kuzminov, V. V., Lobashev, V. M., Novikov, V. M., et al. (1986). Low Background Installation for the ^{136}Xe Double Beta Decay Experiment. *Nucl. Instrum. Meth.* B17, 450–451. doi:10.1016/0168-583X(86)90183-7
- Barabash, A. S., Golubev, A. A., and M., K. B. (1983)
- Barabash, A. S., Novikov, V. M., and M., O. B. (1991). High pressure ionization chamber designed to search for 2β decay of ^{136}Xe . *Nucl. Instr. Meth.* 300, 77
- Bellotti, E. et al. (1989). A Search for Lepton Number Nonconservation in Double Beta Decay of ^{136}Xe . *Phys. Lett.* B221, 209–215. doi:10.1016/0370-2693(89)91500-1
- Bolotnikov, A. and Ramsey, B. (1997). The spectroscopic properties of high-pressure xenon. *Nucl. Instr. Meth.* A396, 360–370
- Bolotnikov, A. and Ramsey, B. (1997). The spectroscopic properties of high-pressure xenon. *Nuclear Instruments and Methods in Physics Research A* 396, 360–370. doi:10.1016/S0168-9002(97)00784-5
- Bolozdynya, A. et al. (1997). A high pressure xenon self-triggered scintillation drift chamber with 3D sensitivity in the range of 20–140 keV deposited energy. *Nuc. Instr. Meth.* A385, 225
- Brunner, T. et al. (2015). An RF-only ion-funnel for extraction from high-pressure gases. *International Journal of Mass Spectrometry* 379, 110–120. doi:10.1016/j.ijms.2015.01.003
- Burghardt, T. P. (2012). Measuring incidence angle for through-the-objective total internal reflection fluorescence microscopy. *Journal of Biomedical Optics* 17, 126007. doi:10.1117/1.JBO.17.12.126007
- Cebrián, S. et al. (2015). Radiopurity assessment of the tracking readout for the NEXT double beta decay experiment. *JINST* 10, P05006. doi:10.1088/1748-0221/10/05/P05006
- Cebrián, S. et al. (2017). Radiopurity assessment of the energy readout for the NEXT double beta decay experiment. *JINST* 12, T08003. doi:10.1088/1748-0221/12/08/T08003
- Charpak, G., Majewski, S., and Sauli, F. (1975). The scintillating drift chamber: A new tool for high accuracy, very high rate particle localization. *Nucl. Instr. Meth.* 126, 381
- Chen, X. et al. (2017). PandaX-III: Searching for neutrinoless double beta decay with high pressure ^{136}Xe gas time projection chambers. *Sci. China Phys. Mech. Astron.* 60, 061011. doi:10.1007/s11433-017-9028-0
- Conde, C. A. N. and Policarpo, A. J. P. L. (1967). A gas proportional scintillation counter. *Nucl. Instr. Meth.* 53, 7–12
- Danilov, M. et al. (2000). Detection of very small neutrino masses in double beta decay using laser tagging. *Physics Letters* B480, 12–18. doi:10.1016/S0370-2693(00)00404-4
- De'Munari, G. and Mambriani, G. (1961). *Suppl. Nuovo Cimento* 19
- De'Munari, G. and Mambriani, G. (1976). A cloud chamber triggered by the electroluminescence of its he+xe filling mixture: a new instrument for investigating double beta-decay. *Nuovo Cimento* 33A, 299
- Fano, U. (1947). Ionization yield of radiations. ii. the fluctuations of the number of ions. *Phys. Rev.* 72, 26–29. doi:10.1103/PhysRev.72.26
- Felkai, R., Monrabal, F., Gonzalez-Díaz, D., Sorel, M., López-March, N., Gómez-Cadenas, J. J., et al. (2018). Helium-Xenon mixtures to improve topological signature in high pressure gas Xenon TPCs. *Nucl. Instrum. Meth.* A905, 82–90. doi:10.1016/j.nima.2018.07.013
- Fernandes, L. M. P. et al. (2010). Primary and secondary scintillation measurements in a xenon Gas Proportional Scintillation Counter. *JINST* 5, P09006. doi:10.1088/1748-0221/5/09/P09006
- Ferrario, P. et al. (2016). First proof of topological signature in the high pressure xenon gas TPC with electroluminescence amplification for the NEXT experiment. *JHEP* 01, 104. doi:10.1007/JHEP01(2016)104

- Fukugita, M. and Yanagida, T. (1986). Baryogenesis without grand unification. *Phys. Lett. B* 174, 45–47. doi:10.1016/0370-2693(86)91126-3
- Gando, A., Gando, Y., Hachiya, T., Hayashi, A., Hayashida, S., Ikeda, H., et al. (2016a). Publisher’s Note: Search for Majorana Neutrinos Near the Inverted Mass Hierarchy Region with KamLAND-Zen [Phys. Rev. Lett. 117, 082503 (2016)]. *Phys. Rev. Lett.* 117, 109903. doi:10.1103/PhysRevLett.117.109903
- Gando, A., Gando, Y., Hachiya, T., Hayashi, A., Hayashida, S., Ikeda, H., et al. (2016b). Search for Majorana Neutrinos Near the Inverted Mass Hierarchy Region with KamLAND-Zen. *Phys. Rev. Lett.* 117, 082503. doi:10.1103/PhysRevLett.117.082503
- Gehring, A. et al. (2016). Research and development of ion surfing {RF} carpets for the cyclotron gas stopper at the {NSCL}. *Nuclear Instruments and Methods in Physics Research Section B: Beam Interactions with Materials and Atoms* 376, 221 – 224. doi:https://doi.org/10.1016/j.nimb.2016.02.012. Proceedings of the {XVIIth} International Conference on Electromagnetic Isotope Separators and Related Topics (EMIS2015), Grand Rapids, MI, U.S.A., 11-15 May 2015
- Gomez-Cadenas, J. (2018). Status of NEXT and prospects for a future Next Array apparatus with Improved Capabilities (NAUSICAA). *PoS NEUTEL2017*, 032
- Gómez Cadenas, J. J., Martín-Albo, J., Mezzetto, M., Monrabal, F., and Sorel, M. (2012). The Search for Neutrinoless Double Beta Decay. *Riv. Nuovo Cim* 35, 29–98
- Gonzalez-Diaz, D., Monrabal, F., and Murphy, S. (2018). Gaseous and dual-phase time projection chambers for imaging rare processes. *Nucl. Instrum. Meth.* A878, 200–255. doi:10.1016/j.nima.2017.09.024
- Gonzalez-Diaz, D. et al. (2015). Accurate γ and MeV-electron track reconstruction with an ultra-low diffusion Xenon/TMA TPC at 10 atm. *Nucl. Instrum. Meth.* A804, 8–24. doi:10.1016/j.nima.2015.08.033
- Granena, F. et al. (2009). NEXT, a HPGXe TPC for neutrinoless double beta decay searches
- Green, A. E. S. (1957). Single electron shakeoff probability following the beta decay of krypton. *Physical Review* 107, 1646–1650. doi:10.1103/PhysRev.107.1646
- Habuchi, S., Ando, R., Dedecker, P., Verheijen, W., Mizuno, H., Miyawaki, A., et al. (2005). Reversible single-molecule photoswitching in the gfp-like fluorescent protein dropna. *Proceedings of the National Academy of Sciences of the United States of America* 102, 9511–9516. doi:10.1073/pnas.0500489102
- Han, K. (2017). PandaX-III: Searching for Neutrinoless Double Beta Decay with High Pressure Gaseous Time Projection Chambers. In *15th International Conference on Topics in Astroparticle and Underground Physics (TAUP 2017) Sudbury, Ontario, Canada, July 24-28, 2017*
- Henriques, C. A. O. et al. (2017). Secondary scintillation yield of xenon with sub-percent levels of CO₂ additive for rare-event detection. *Phys. Lett. B* 773, 663–671. doi:10.1016/j.physletb.2017.09.017
- Iqbal, M. Z., Henrikson, H. E., Mitchell, L. W., O’Callaghan, B. M. G., Thomas, J., and Wong, H. T. (1987). Design and Construction of a High Pressure Xenon Time Projection Chamber. *Nucl. Instrum. Meth.* A259, 459–465. doi:10.1016/0168-9002(87)90827-8
- Jones, B. J. P., McDonald, A. D., and Nygren, D. R. (2016). Single Molecule Fluorescence Imaging as a Technique for Barium Tagging in Neutrinoless Double Beta Decay. *JINST* 11, P12011. doi:10.1088/1748-0221/11/12/P12011
- Lorca, D. et al. (2014). Characterisation of NEXT-DEMO using xenon K α X-rays. *JINST* 9, P10007. doi:10.1088/1748-0221/9/10/P10007
- Lu, Y. and Paige, M. F. (2007). An ensemble and single-molecule fluorescence spectroscopy investigation of calcium green 1, a calcium-ion sensor. *Journal of Fluorescence* 17, 739–748. doi:10.1007/s10895-007-0185-1

- Luscher, R. et al. (1998). Search for $\beta\beta$ decay in Xe-136: New results from the Gotthard experiment. *Phys. Lett. B* 434, 407–414. doi:10.1016/S0370-2693(98)00906-X
- Majorana, E. (1937). Theory of the Symmetry of Electrons and Positrons. *Nuovo Cim.* 14, 171–184
- Martín-Albo, J. (2015). *The NEXT experiment for neutrinoless double beta decay searches*. Ph.D. thesis, Valencia U., IFIC
- Martín-Albo, J. et al. (2016). Sensitivity of NEXT-100 to Neutrinoless Double Beta Decay. *JHEP* 05, 159. doi:10.1007/JHEP05(2016)159
- Martínez-Lema, G. et al. (2018). Calibration of the NEXT-White detector using ^{83m}Kr decays. *JINST* 13, P10014. doi:10.1088/1748-0221/13/10/P10014
- McDonald, A. D. et al. (2018). Demonstration of Single Barium Ion Sensitivity for Neutrinoless Double Beta Decay using Single Molecule Fluorescence Imaging. *Phys. Rev. Lett.* 120, 132504. doi:10.1103/PhysRevLett.120.132504
- Moe, M. K. (1991). New approach to the detection of neutrinoless double beta decay. *Physical Review* C44, 931–934. doi:10.1103/PhysRevC.44.931
- Mong, B. et al. (2015). Spectroscopy of Ba and Ba⁺ deposits in solid xenon for barium tagging in nEXO. *Physical Review* A91, 022505. doi:10.1103/PhysRevA.91.022505
- Monrabal, F. et al. (2018). The Next White (NEW) Detector. *arXiv: 1804.02409*. Accepted by JINST
- Monteiro, C. M. B. and others. (2007). Secondary scintillation yield in pure xenon. *Journal of Instrumentation* 2, P05001
- Muñoz Vidal, J. (2018). *The NEXT path to neutrino inverse hierarchy*. Ph.D. thesis, Universitat de València, Av. de Blasco Ibáñez, 13, 46010 Valencia, Spain
- Nakajima, Y., Goldschmidt, A., Matis, H. S., Nygren, D., Oliveira, C., and Renner, J. (2015). Measurement of scintillation and ionization yield with high-pressure gaseous mixtures of Xe and TMA for improved neutrinoless double beta decay and dark matter searches. *J. Phys. Conf. Ser.* 650, 012012. doi:10.1088/1742-6596/650/1/012012
- Nakamura, K. et al. (2017). AXEL—a high pressure xenon gas TPC for neutrinoless double beta decay search. *Nucl. Instrum. Meth.* A845, 394–397. doi:10.1016/j.nima.2016.06.083
- Novella, P. et al. (2018). Measurement of radon-induced backgrounds in the NEXT double beta decay experiment. *JHEP* 10, 112. doi:10.1007/JHEP10(2018)112
- Nygren, D. (2007). Optimal detectors for WIMP and $0\nu\beta\beta$ searches: Identical high-pressure xenon gas TPCs? *Nucl. Instrum. Meth.* A581, 632–642
- Nygren, D. (2009). High-pressure xenon gas electroluminescent TPC for $0 - \nu \beta\beta$ -decay search. *Nucl. Instrum. Meth.* A603, 337–348. doi:10.1016/j.nima.2009.01.222
- Nygren, D. R. (1974). The Time Projection Chamber: A New 4 pi Detector for Charged Particles. *eConf* C740805, 58
- Nygren, D. R. (2014). The Biochemistry of ^{136}Xe . 7th international symposium on large TPCs for low-energy rare event detection
- Oliveira, C. A. B., Sorel, M., Martín-Albo, J., Gomez-Cadenas, J. J., Ferreira, A. L., and Veloso, J. F. C. A. (2011). Energy Resolution studies for NEXT. *JINST* 6, P05007. doi:10.1088/1748-0221/6/05/P05007
- Renner, J., Farbin, A., Muñoz Vidal, J., Benlloch-Rodriguez, J. M., Botas, A., Ferrario, P., et al. (2017). Background rejection in NEXT using deep neural networks. *JINST* 12, T01004–T01004. doi:10.1088/1748-0221/12/01/T01004
- Renner, J. et al. (2018). Initial results on energy resolution of the NEXT-White detector. *JINST* 13, P10020. doi:10.1088/1748-0221/13/10/P10020
- Simón, A. et al. (2018). Electron drift properties in high pressure gaseous xenon. *JINST* 13, P07013

- Sinclair, D. et al. (2011). Prospects for Barium Tagging in Gaseous Xenon. *Journal of Physics Conference Series* 309, 012005. doi:10.1088/1742-6596/309/1/012005
- [Dataset] Stuurman, N. and Vale, R. (2006). Imaging single molecules using total internal reflection fluorescence microscopy
- Thomas, D., Tovey, S., Collins, T., Bootman, M., Berridge, M., and Lipp, P. (2000). A comparison of fluorescent Ca^{2+} indicator properties and their use in measuring elementary and global Ca^{2+} signals. *Cell calcium* 28, 213–223
- Trindade, A. M. et al. (2018). Study of the loss of xenon scintillation in xenon-trimethylamine mixtures. *Nucl. Inst. Meth.* 905, 23
- Wong, H. T. et al. (1991). First 0ν half-life limit from the Gotthard xenon time projection chamber. *J. Phys. G17*, S165–S172. doi:10.1088/0954-3899/17/S/017

FIGURE CAPTIONS

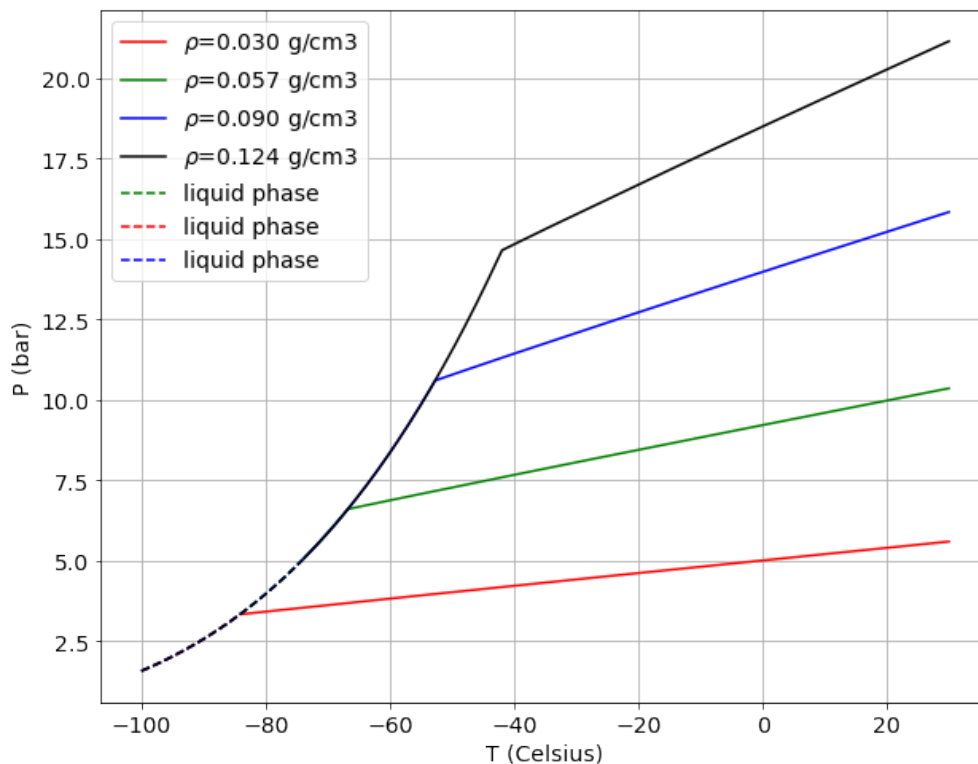


Figure 1. Isochoric curves for xenon at different densities.

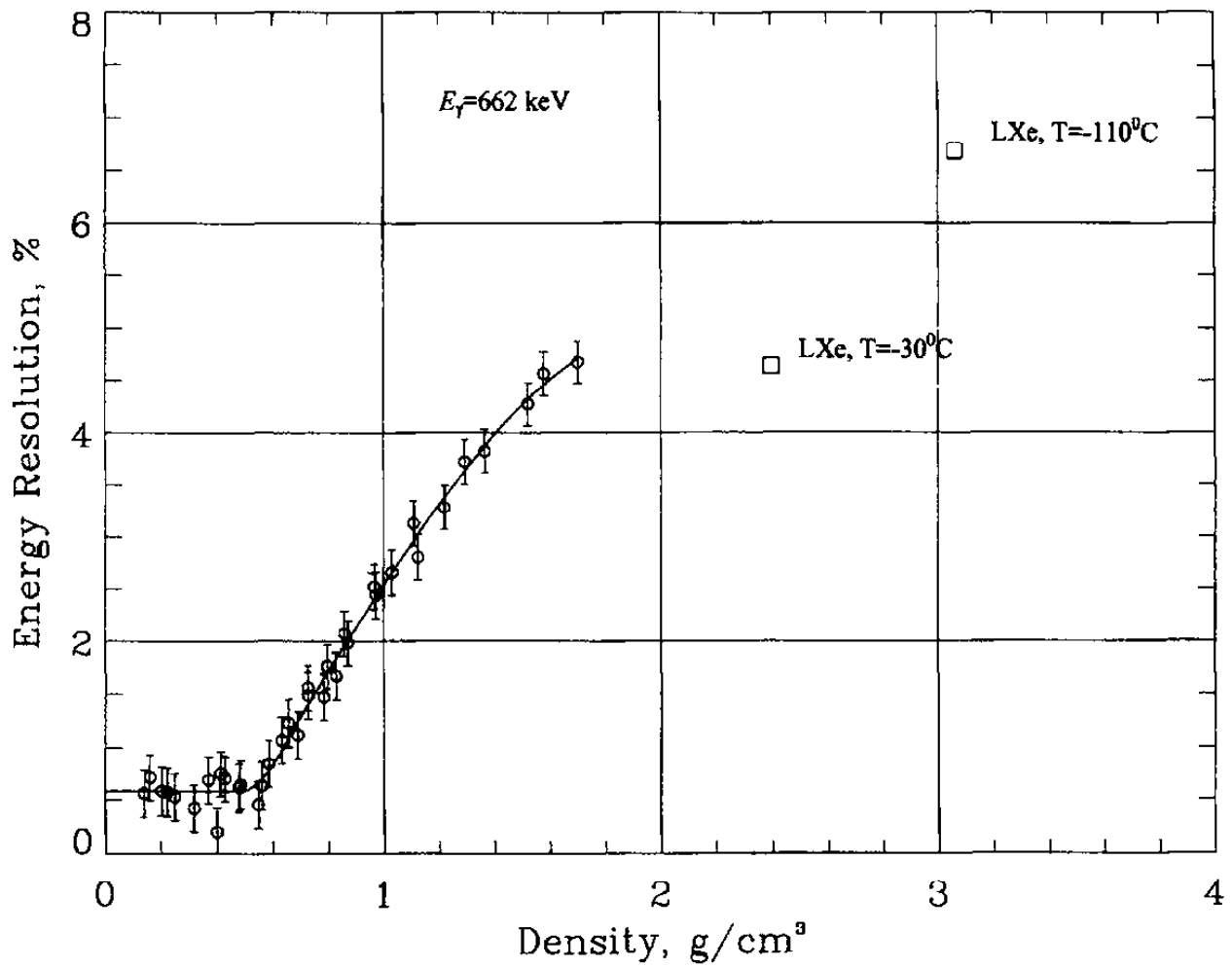


Figure 2. The energy resolution (FWHM) is shown for ¹³⁷Cs 662 keV gamma rays, as a function of xenon density, for the ionization signal only. Reproduced from [Bolotnikov and Ramsey, 1997].

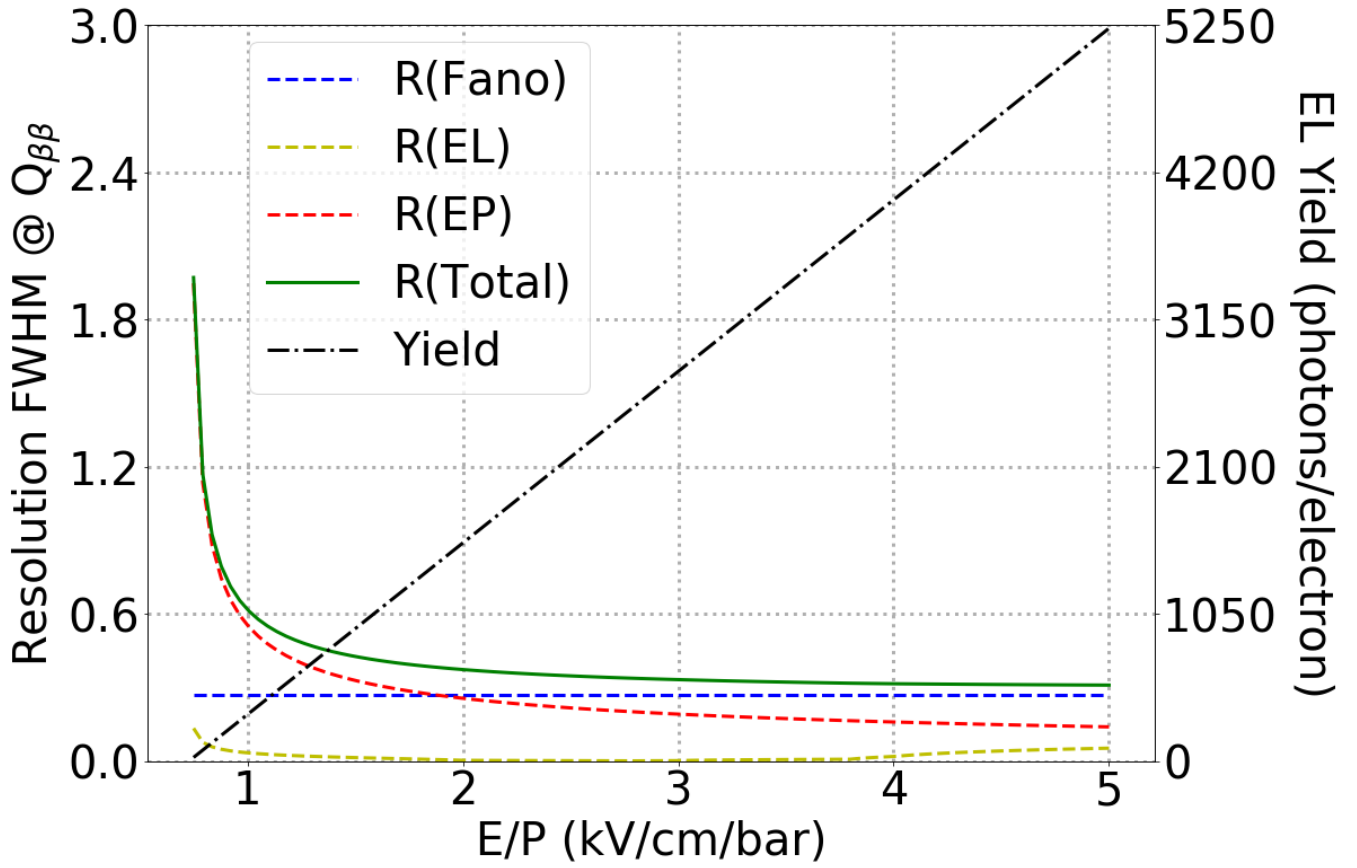


Figure 3. Energy resolution terms and EL yield characteristic of a HPXe-EL TPC as a function of the reduced electric field for an EL gap of 6 mm a value of $k \sim 0.016$ and a pressure of 15 bar.

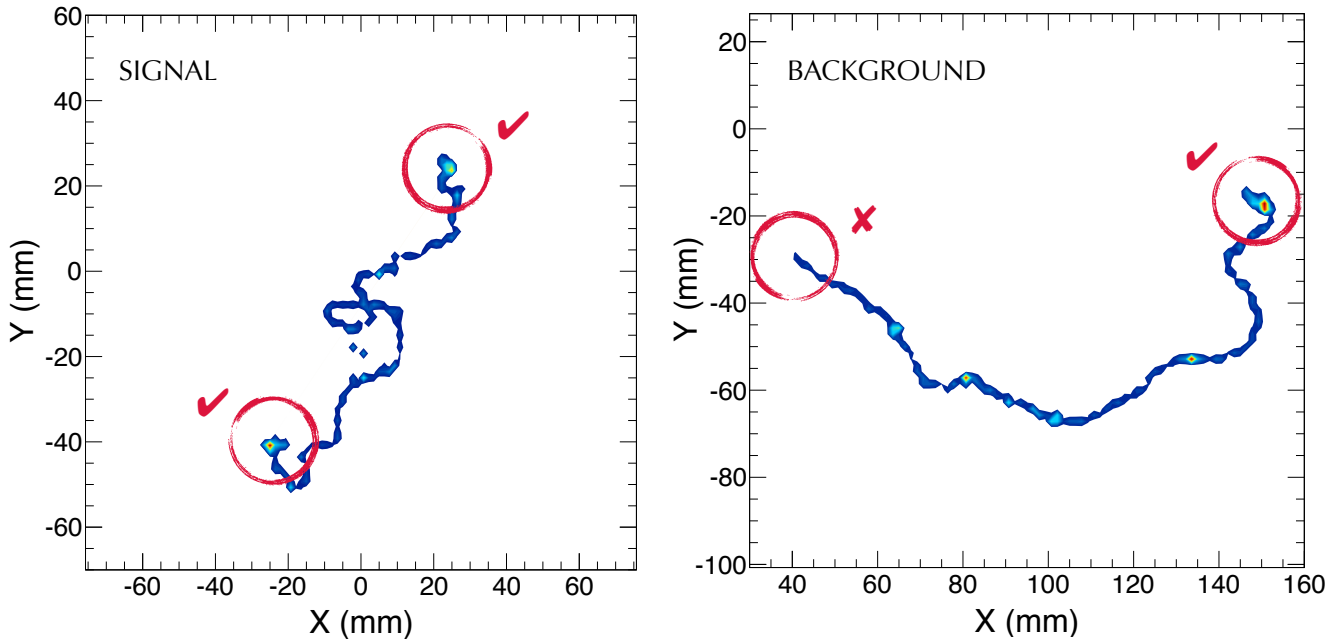


Figure 4. The left panel shows two electrons emitted in a $\beta\beta 0\nu$ decay propagating in HPXe with perfect track reconstruction; the right panel shows a single background electron produced by a photoelectric interaction from a ^{214}Bi gamma of energy very close to $Q_{\beta\beta}$. While the energy of the background electron could enter the ROI, the topology of the latter is different from the former. A $\beta\beta 0\nu$ event results in two electrons which are ended in two blobs of energy as the electron deposit suddenly its energy near the end-of-the-ionization path (Bragg peak). In the case of a background electron there is only a single blob. Figure from [Martín-Albo et al., 2016]

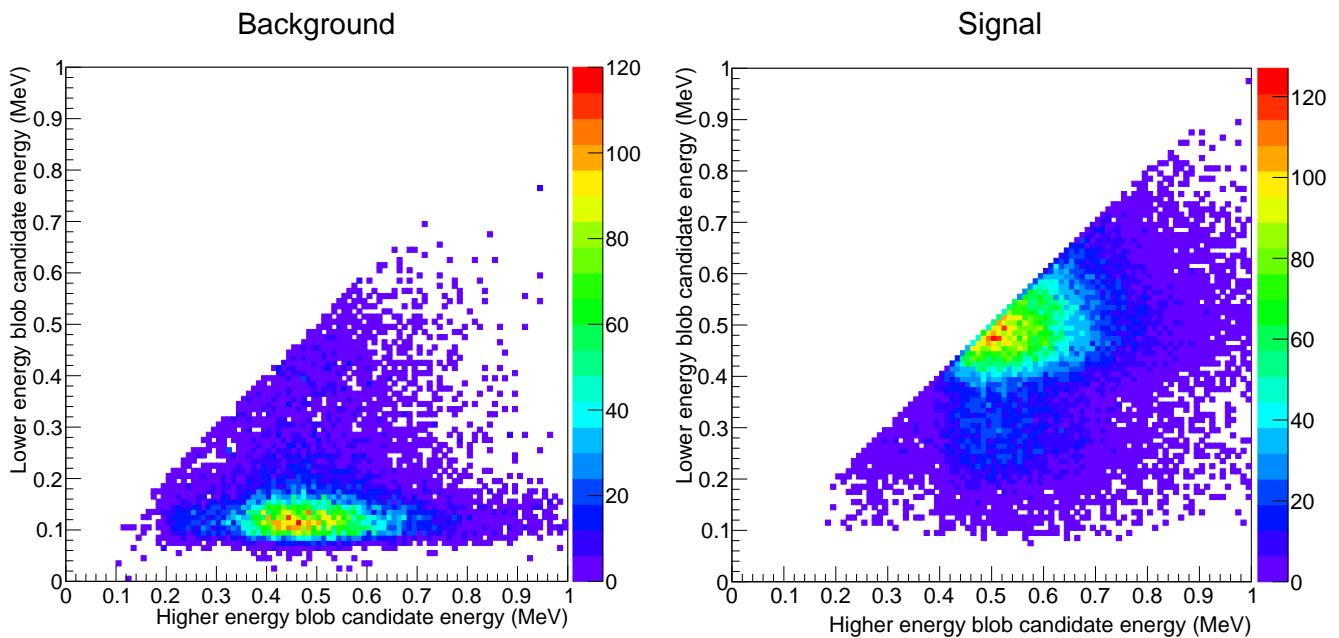


Figure 5. The left panel shows the energy of the blob of less energy versus the energy of the blob of high energy for a background electron propagating in a HPXe TPC —perfect track reconstruction—, while the right plot shows the same plot of the 2 electrons produced in a $\beta\beta 0\nu$ propagating under the same conditions. In the first case the energy of the lower energy blob is much smaller than the energy of the higher energy blob, in the second case both are roughly the same.

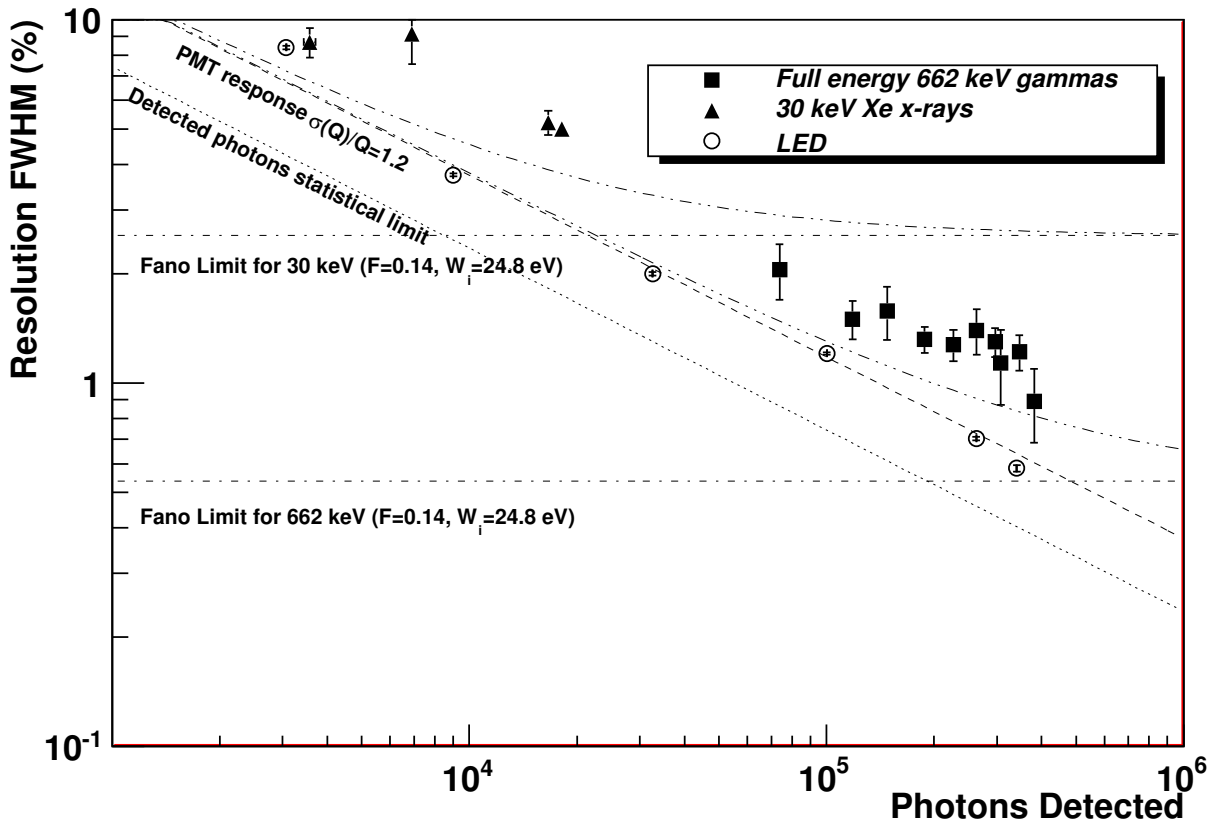


Figure 6. Energy resolution measured by NEXT-DBDM: Data points show the measured energy resolution for 662 keV gammas (squares), ~ 30 keV xenon X-rays (triangles) and LED light pulses (circles) as a function of the number of photons detected. The expected resolution including the intrinsic Fano factor, the statistical fluctuations in the number of detected photons and the PMT charge measurement variance is shown for X-rays (dot dot dashed) and for 662 keV gammas (dot dot dot dashed). Resolutions for the 662 keV peak were obtained from 15 bar data runs while X-ray resolutions we obtained from 10 bar runs. Figure from [Álvarez et al., 2012a].

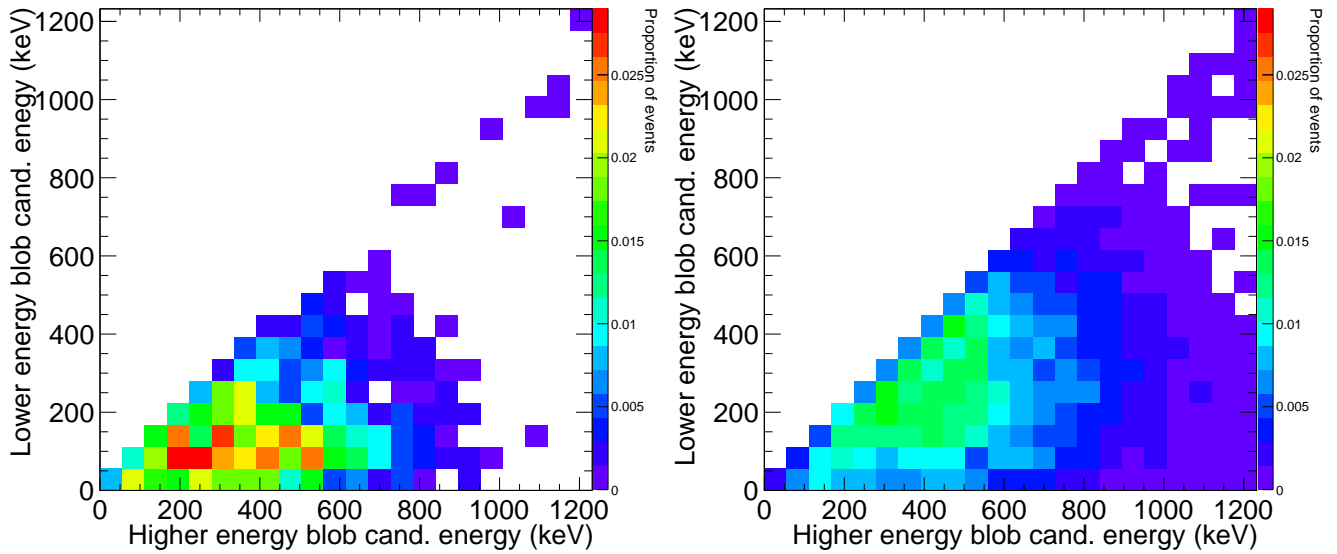


Figure 7. Energy distribution of the blobs at the end-point of single electrons coming from ^{22}Na decays (left) and tracks (mostly electron-positron pairs) coming from the ^{208}Tl double escape peak (right). Figure from [Ferrario et al., 2016].

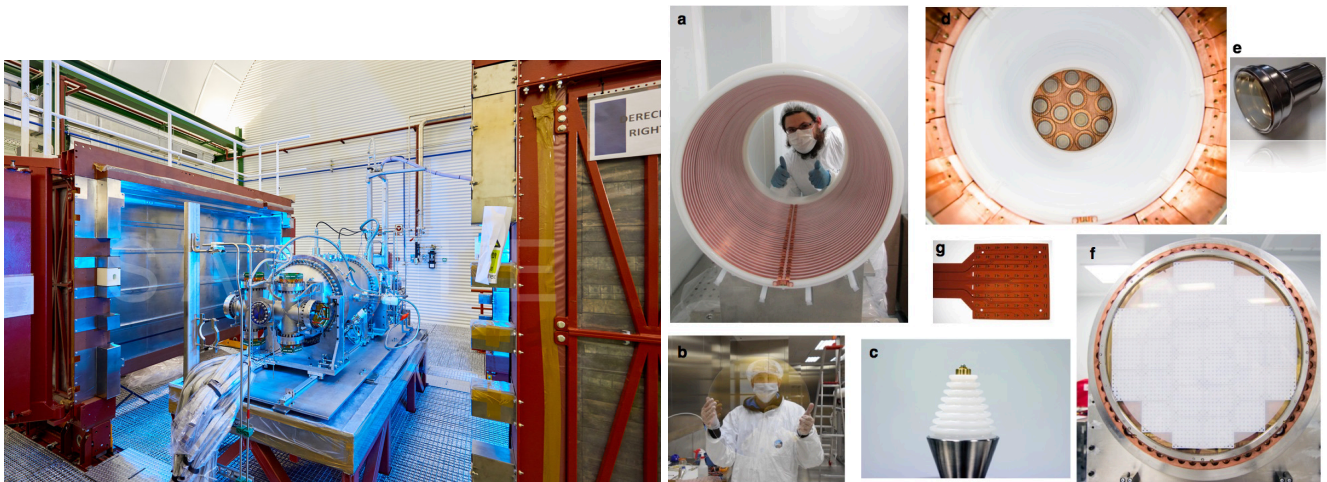


Figure 8. Left: the NEXT-White detector at the LSC. Right: a selection of the main subsystems of NEXT-White: a) the field cage; b) the anode plate; c) high voltage feedthrough; d) energy plane; e) PMTs used in the energy plane; f) tracking plane; g) kapton boards composing the tracking plane.

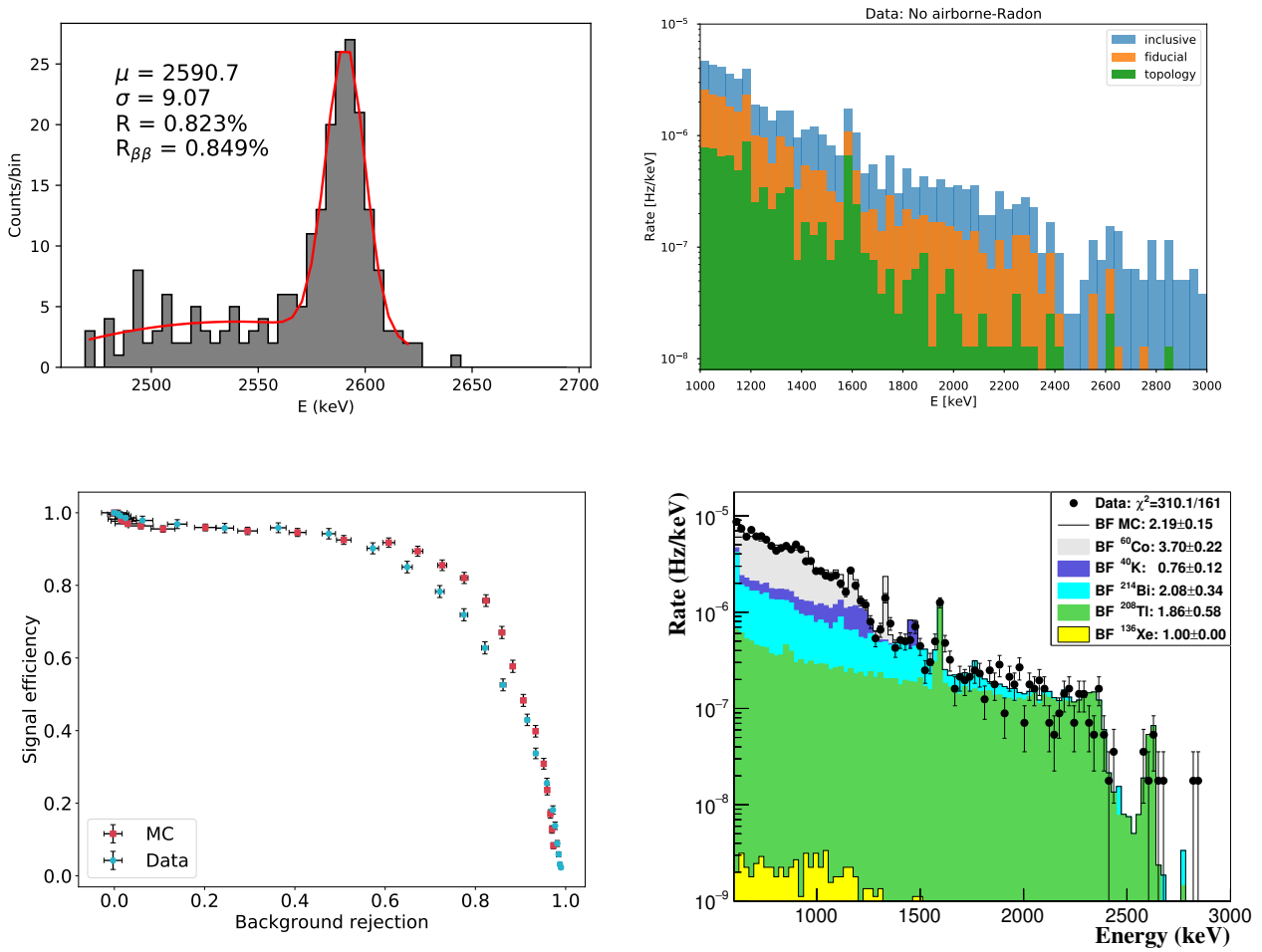


Figure 9. A selection of the preliminary results obtained by NEXt-White. See text for details.

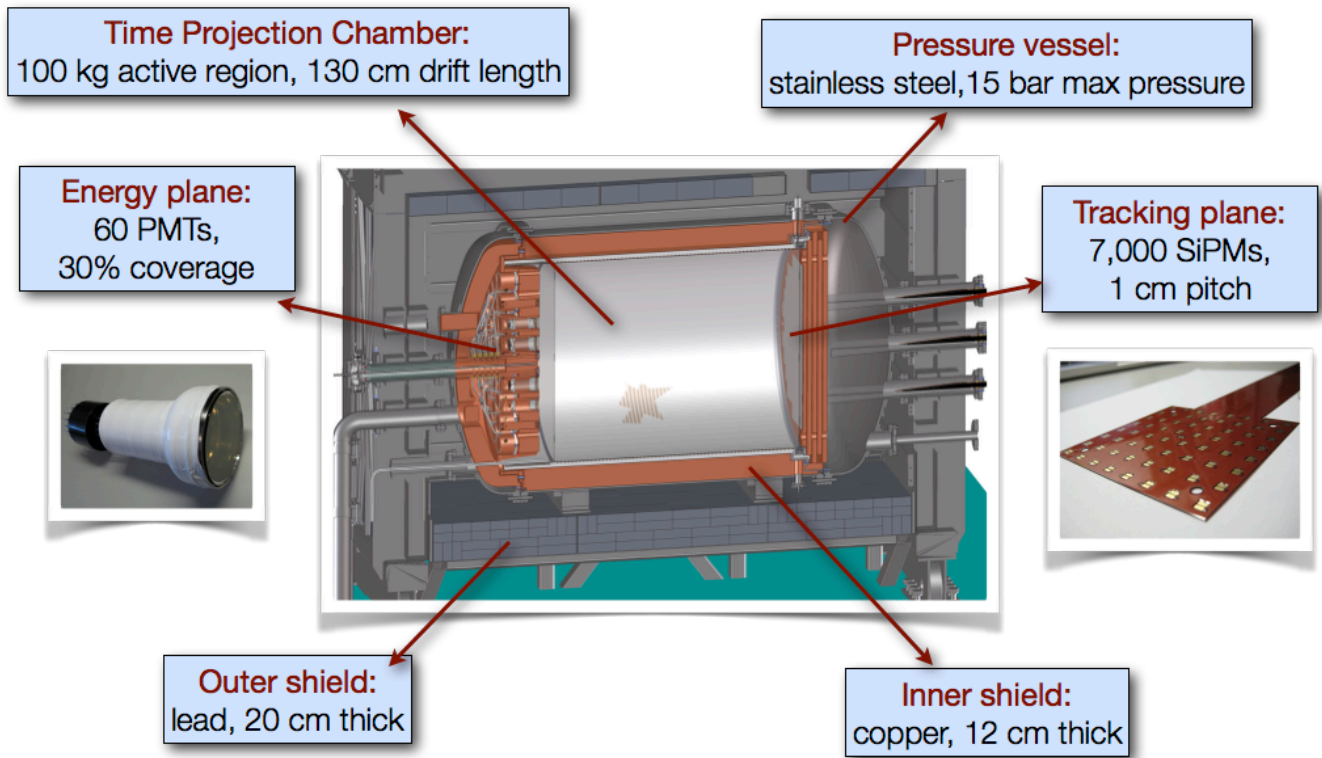


Figure 10. The NEXT-100 detector.

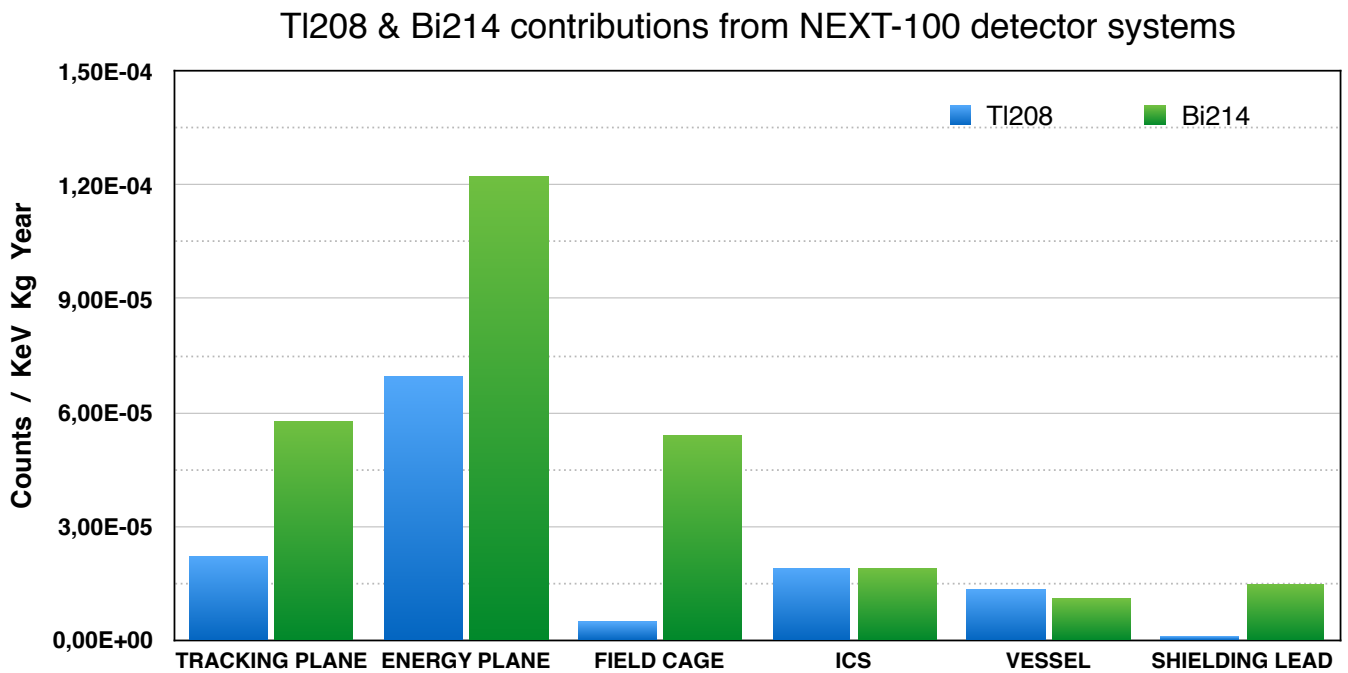


Figure 11. NEXT-100 background budget after selection. Figure from [Muñoz Vidal, 2018].

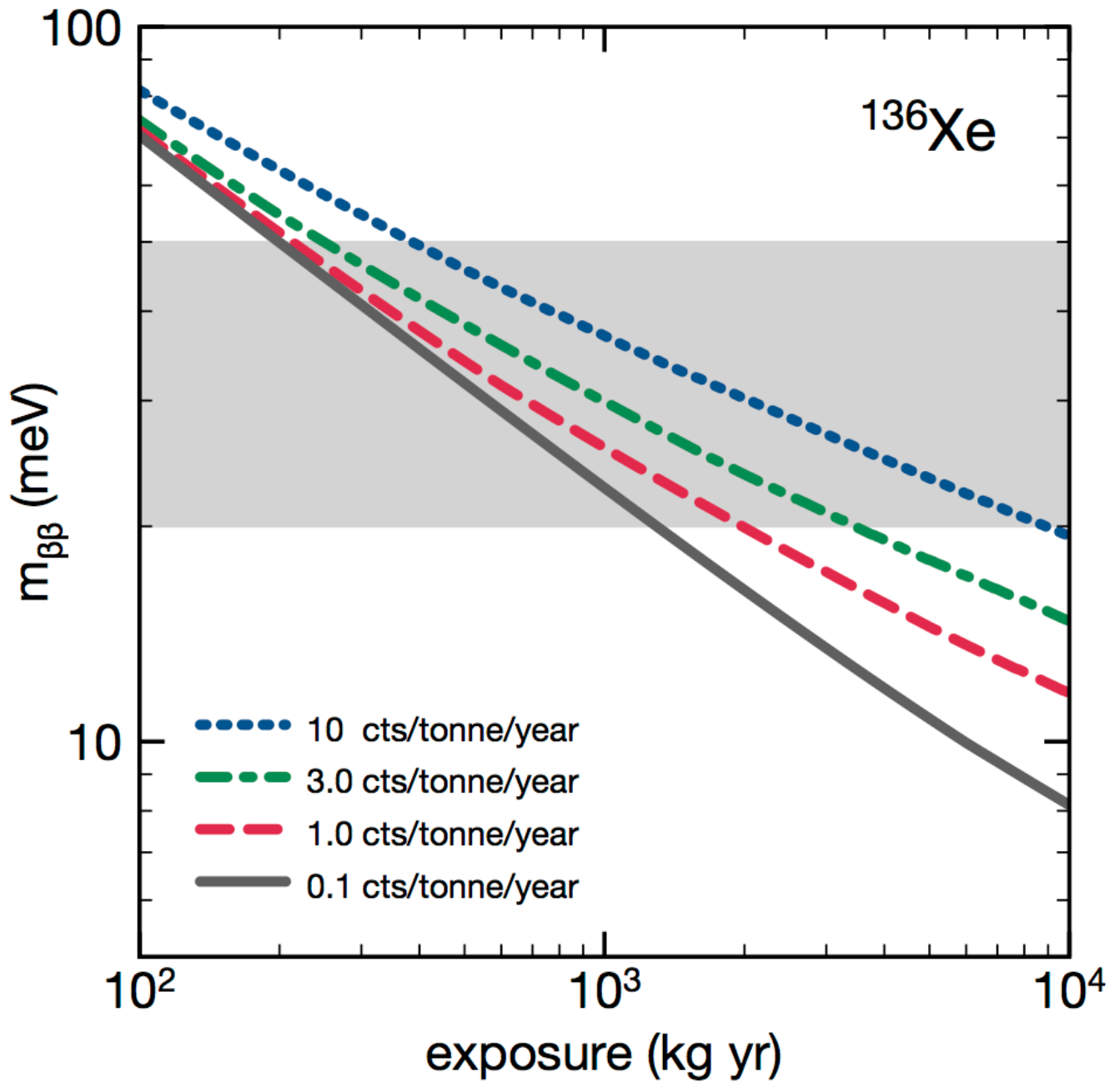


Figure 12. Sensitivity of a fully efficient ^{136}Xe experiment as a function of the exposure, for different background rates [Martín-Albo, 2015].

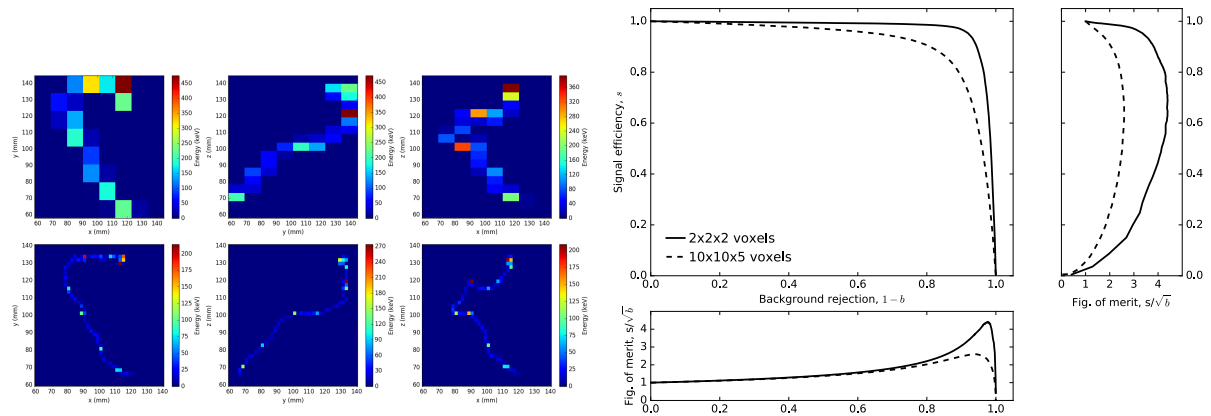


Figure 13. Left: The three projections of a reconstructed Monte Carlo electron in NEX-100 (top panels) and NEX-2.0 (bottom panels). Right: Signal efficiency versus background rejection provided by the topological signature in both detectors. See text for details. Reproduced from [Renner et al., 2017].

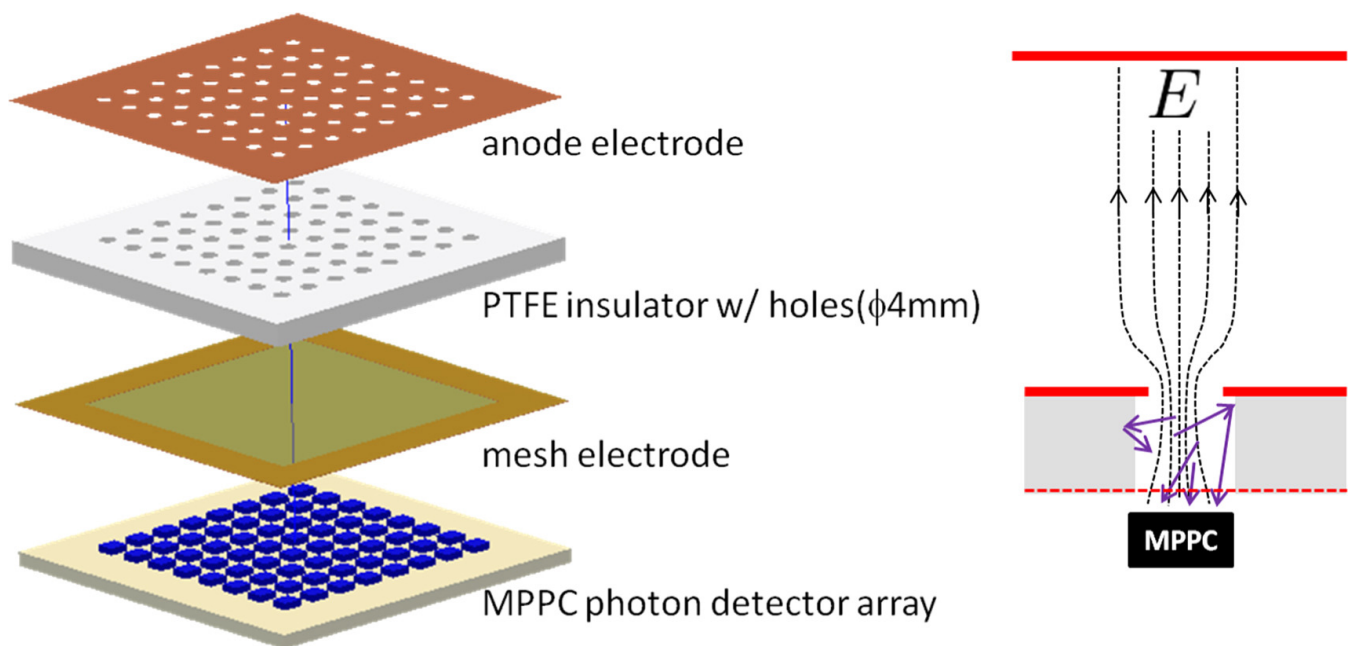


Figure 14. The ELCC concept. Figure from [Nakamura et al., 2017].

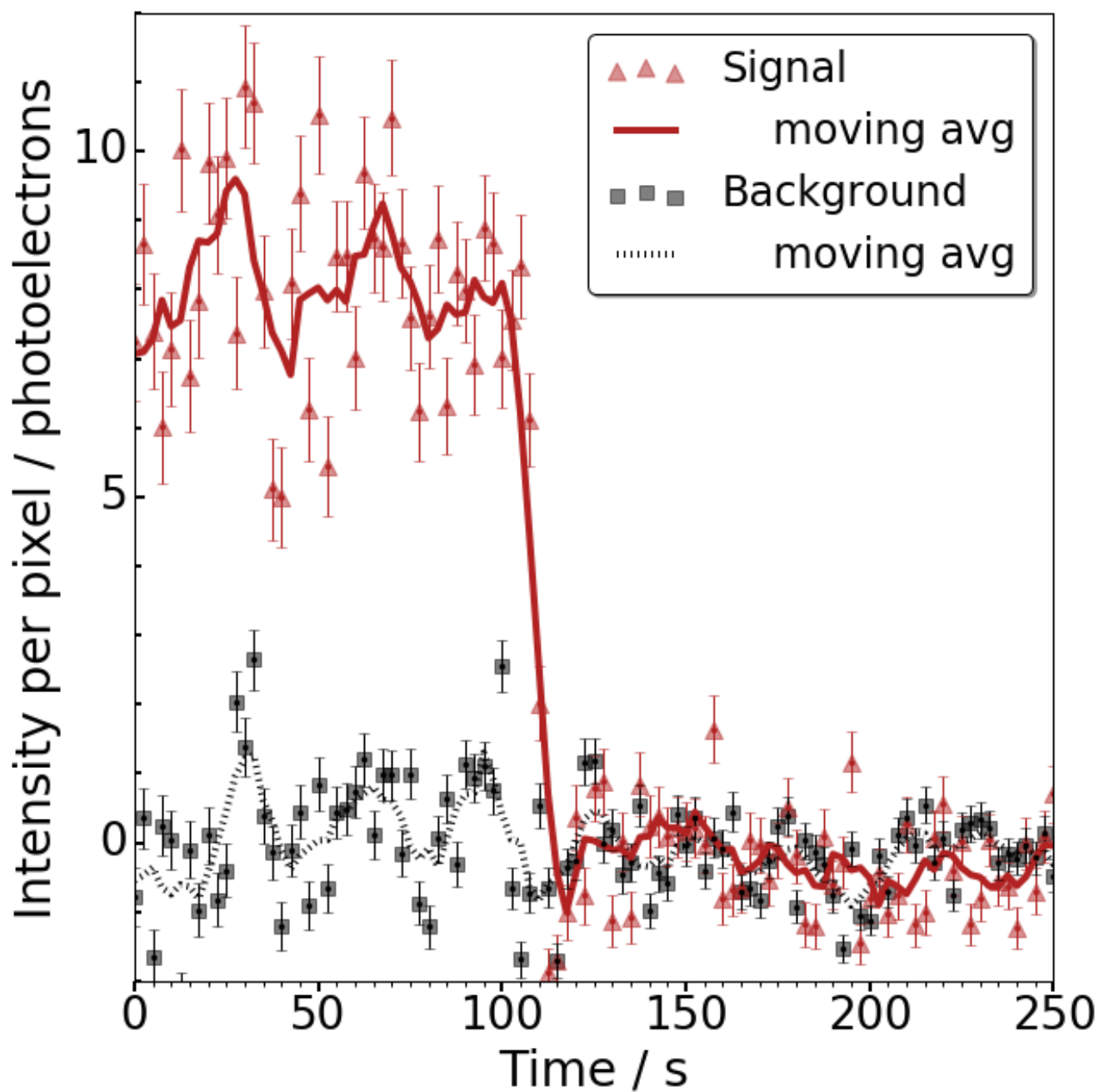


Figure 15. Fluorescence trajectory for one candidate in a barium-spiked sample. “Signal” shows the average activity in 5×5 pixels centered on the local maximum. “Background” shows the average in the 56 surrounding. The single step photo-bleach is characteristic of single molecule fluorescence. Figure from [McDonald et al., 2018].